Vacuum Stability in Inert Higgs Doublet Model with Right-handed Neutrinos

Priyotosh Bandyopadhyay,[a] **P. S. Bhupal Dev,**[b] **Shilpa Jangid,**[a] **Arjun Kumar**[c]

[a]*Indian Institute of Technology Hyderabad, Kandi, Sangareddy-502287, Telengana, India*

[b]*Department of Physics and McDonnell Center for the Space Sciences, Washington University, St. Louis, MO 63130, USA*

[c]*Indian Institute of Technology Delhi, Hauzkhas, New Delhi-110016, Delhi, India*

E-mail: bpriyo@iith.ac.in, bdev@wustl.edu, ph19resch02006@iith.ac.in, Arjun.Kumar@physics.iitd.ac.in

ABSTRACT: We analyze the vacuum stability in the inert Higgs doublet extension of the Standard Model (SM), augmented by right-handed neutrinos (RHNs) to explain neutrino masses at tree level by the seesaw mechanism. We make a comparative study of the high- and low-scale seesaw scenarios and the effect of the Dirac neutrino Yukawa couplings on the stability of the Higgs potential. Bounds on the scalar quartic couplings and Dirac Yukawa couplings are obtained from vacuum stability and perturbativity considerations. The regions corresponding to stability, metastability and instability of the electroweak vacuum are identified. These theoretical constraints give a very predictive parameter space for the couplings and masses of the new scalars and RHNs which can be tested at the LHC and future colliders. The lightest non-SM neutral CP-even/odd scalar can be a good dark matter candidate and the corresponding collider signatures are also predicted for the model.

KEYWORDS: Beyond Standard Model, Extended Higgs Sector, Vacuum Stability, Dark Matter, Large Hadron Collider

Contents

1   Introduction

The last missing piece of the Standard Model (SM) particle spectrum was found in 2012 with the discovery of a SM-like Higgs boson with a mass of about 125 GeV at the Large Hadron Collider (LHC) [1, 2], followed by increasingly-precise measurements [3–6] on its spin, parity, and couplings to SM particles, all of which are consistent within the uncertainties with those expected in the SM [7]. On the other hand, there are ample experimental evidences, ranging from observed dark matter (DM) relic density and matter-antimatter asymmetry in the universe to nonzero neutrino masses, that necessitate an extension of the SM, often involving the scalar sector. Moreover, from the theoretical viewpoint, it is known that the SM by itself cannot ensure the absolute stability of the electroweak (EW) vacuum up to the

Planck scale [8–11].[1] An extended scalar sector with additional bosonic degrees of freedom can alleviate the stability issue, by compensating for the destabilizing effect of the top-quark Yukawa coupling on the renormalization group (RG) evolution of the SM Higgs quartic coupling. The issue of vacuum stability in presence of additional scalars has been extensively studied in the literature. An incomplete list of models include SM-singlet scalar models [19–25], Two-Higgs doublet models (2HDM) [26–31], type-II seesaw models with $SU(2)_L$-triplet scalars [32–38], $U(1)$ extensions [39–45], left-right symmetric models [46–48], universal seesaw models [49, 50], Zee-Babu model [51, 52], models with Majorons [53, 54], axions [22, 55], moduli [56, 57], scalar leptoquarks [58] or higher color-multiplet scalars [59, 60], as well as various super-symmetric models [61–71]. In contrast, additional fermions typically aggravate the EW vacuum stability, as shown e.g. in type-I [72–78], III [79–82], linear [83] and inverse [84, 85] seesaw scenarios, fermionic EW-multiplet DM models [86–89], or models with vectorlike fermions [90, 91].

As alluded to above, nonzero neutrino masses provide a strong motivation for beyond the SM physics. Arguably, the simplest paradigm to account for tiny neutrino masses is the so-called type-I seesaw mechanism with additional right-handed heavy Majorana neutrinos [92–96]. However, it comes with the additional Dirac Yukawa couplings which contribute negatively to the RG running of the SM Higgs quartic coupling, thus aggravating the vacuum stability problem. One way to alleviate the situation is by adding extra scalars [97–100] which compensate for the destabilizing effect of the right-handed neutrinos (RHNs). Following this approach, we consider in this paper an inert 2HDM [101, 102] with the addition of RHNs for seesaw mechanism. The neutral component of the inert doublet is stable due to a discrete Z_2 symmetry and can be identified as the DM candidate [102–109].[2] Though the second Higgs doublet remains inert as far as the EW symmetry breaking is concerned, it plays an important role in deciding the stability of the EW minimum for given Dirac neutrino Yukawa couplings. For sizable quartic couplings in the 2HDM sector, we find that the effect of large Dirac Yukawa couplings from the RHN sector can be compensated to keep the EW vacuum stable all the way up to the Planck scale. We also discuss the collider phenomenology of this model, and in particular, new exotic decay modes of the RHNs involving the heavy Higgs bosons.

The rest of this article is organized as follows: In Section 2 we briefly review the inert 2HDM with RHNs. In Section 3, the RG running effects are discussed in the

---

[1]This is not a problem per se, as for the current best-fit values of the SM Higgs and top-quark masses [12], the EW vacuum is metastable in the SM with a lifetime much longer than the age of the universe [13]. However, absolute stability is desired, for instance, for the success of minimal Higgs inflation [14] (see Ref. [15] for a way around, though). Moreover, Planck-scale higher-dimensional operators can have a large effect to render the metastability prediction unreliable in the SM [16–18].

[2]A variant of this model with an additional scalar singlet was considered in Refs. [99, 100] to obtain a multi-component DM scenario.

context of perturbativity. In Section 4, the stability of the EW vacuum has been studied in detail as a function of the Yukawa couplings. Some LHC phenomenology is touched upon in Section 5. Our conclusions are given in Section 6. For completeness, we give the expressions for two-loop beta functions used in our analysis in Appendix A.

2 The Model

We extend the SM by adding another $SU(2)_L$-doublet scalar field and three RHNs which are singlets under the SM gauge group. The scalar sector of the model is discussed in Section 2.1. For the vacuum stability analysis, we consider two different scenarios for the RHNs, viz., a canonical type-I seesaw with small Yukawa couplings and an inverse seesaw with large Yukawa couplings, which are discussed in Section 2.2.

2.1 The Scalar Sector

The scalar sector of this model consists of two $SU(2)_L$-doublet scalars Φ_1 and Φ_2 with the same hypercharge 1/2:

$$\Phi_1 = \begin{pmatrix} G^+ \\ h + iG^0 \end{pmatrix}, \qquad \Phi_2 = \begin{pmatrix} H^+ \\ H + iA \end{pmatrix}. \tag{2.1}$$

The tree-level Higgs potential symmetric under the SM gauge group $SU(2)_L \times U(1)_Y$ is given by [110]

$$\begin{aligned} V_{\text{scalar}} &= m_{11}^2 \Phi_1^\dagger \Phi_1 + m_{22}^2 \Phi_2^\dagger \Phi_2 - (m_{12}^2 \Phi_1^\dagger \Phi_2 + \text{H.c}) \\ &\quad + \lambda_1 (\Phi_1^\dagger \Phi_1)^2 + \lambda_2 (\Phi_2^\dagger \Phi_2)^2 + \lambda_3 (\Phi_1^\dagger \Phi_1)(\Phi_2^\dagger \Phi_2) + \lambda_4 (\Phi_1^\dagger \Phi_2)(\Phi_2^\dagger \Phi_1) \\ &\quad + \left[\lambda_5 (\Phi_1^\dagger \Phi_2)^2 + \lambda_6 (\Phi_1^\dagger \Phi_1)(\Phi_1^\dagger \Phi_2) + \lambda_7 (\Phi_2^\dagger \Phi_2)(\Phi_1^\dagger \Phi_2) + \text{H.c} \right], \end{aligned} \tag{2.2}$$

where the mass terms m_{11}^2, m_{22}^2 and the quartic couplings $\lambda_{1,2,3,4}$ are all real, whereas m_{12}^2 and the $\lambda_{5,6,7}$ couplings are in general complex. To avoid the dangerous flavor changing neutral currents at tree-level and to make Φ_2 inert for getting a DM candidate, we impose an additional Z_2 symmetry under which Φ_2 is odd and Φ_1 is even. This removes the m_{12}, λ_6 and λ_7 terms from the potential and Eq. (2.2) reduces to

$$\begin{aligned} V_{\text{scalar}} &= m_{11}^2 \Phi_1^\dagger \Phi_1 + m_{22}^2 \Phi_2^\dagger \Phi_2 + \lambda_1 (\Phi_1^\dagger \Phi_1)^2 + \lambda_2 (\Phi_2^\dagger \Phi_2)^2 \\ &\quad + \lambda_3 (\Phi_1^\dagger \Phi_1)(\Phi_2^\dagger \Phi_2) + \lambda_4 (\Phi_1^\dagger \Phi_2)(\Phi_2^\dagger \Phi_1) + \left[\lambda_5 (\Phi_1^\dagger \Phi_2)^2 + \text{H.c} \right]. \end{aligned} \tag{2.3}$$

The EW symmetry breaking is achieved by giving real vacuum expectation value (VEV) to the first Higgs doublet, i.e

$$\langle \Phi_1 \rangle = \frac{1}{\sqrt{2}} \begin{pmatrix} 0 \\ v \end{pmatrix}, \tag{2.4}$$

with $v \simeq 246$ GeV, whereas the second Higgs doublet, being Z_2-odd, does not take part in symmetry breaking (hence the name 'inert 2HDM').

Using minimization conditions, we express the mass parameter m_{11} in terms of other parameters as follows:

$$m_{11}^2 = -\lambda_1 v^2 \,, \tag{2.5}$$

whereas the physical scalar masses are given by

$$
\begin{aligned}
M_h^2 &= 2\lambda_1 v^2 \,, \\
M_H^2 &= \frac{1}{2}[2m_{22}^2 + v^2(\lambda_3 + \lambda_4 + 2\lambda_5)] \,, \\
M_A^2 &= \frac{1}{2}[2m_{22}^2 + v^2(\lambda_3 + \lambda_4 - 2\lambda_5)] \,, \\
M_{H^\pm}^2 &= m_{22}^2 + \frac{1}{2}v^2\lambda_3 \,.
\end{aligned}
\tag{2.6}
$$

Since Φ_2 is inert, there is no mixing between Φ_1 and Φ_2 and the gauge eigenstates are same as the mass eigenstates for the Higgs bosons. The Z_2-symmetry prevents any such mixing through the Higgs portal. In this scenario, the second Higgs doublet does not couple to fermions. Moreover, we get two CP even neutral Higgs bosons h and H, where h is identified as the SM-like Higgs boson of mass 125 GeV discovered at the LHC. We also get one pseudoscalar Higgs boson A and a pair of charged Higgs bosons $H^\pm$. Notice from Eq. (2.6) that the heavy Higgs bosons H, A and $H^\pm$ are nearly degenerate. Depending upon the sign of λ_5 one of scalars between H and A can be a cold DM candidate. Since all the physical Higgs bosons except h are Φ_2-type, i.e., Z_2-odd, this also restricts their decay modes.

2.2 The Fermion Sector

In the fermion sector, we just add SM gauge-singlet RHNs to the SM particle content to generate tree-level neutrino mass via seesaw mechanism. In the canonical type-I seesaw, we just add three RHNs N_{R_i}, where $i = 1, 2, 3$ and the relevant part of the Yukawa Lagrangian is given by

$$\mathcal{L}_{\mathrm{I}} = i\overline{N}_{R_i}\slashed{\partial}N_{R_i} - \left(Y_{N_{ij}}\overline{L}_i\widetilde{\Phi}_1 N_{R_j} + \frac{1}{2}\overline{N}_{R_i}^c M_{R_i} N_{R_i} + \mathrm{H.c.}\right) , \tag{2.7}$$

where $L \equiv (\nu, \ell)_L$ is the SM lepton doublet, $\widetilde{\Phi}_1 = i\sigma_2\Phi_1^\star$ (with σ_2 being the second Pauli matrix), $N_R^c \equiv N_R^\mathsf{T} C^{-1}$ (with C being the charge conjugation matrix), Y_N is the 3×3 Yukawa matrix and M_R is the 3×3 diagonal mass matrix for RHNs.

After EW symmetry breaking by the VEV of Φ_1, the Y_N couplings generate the Dirac mass terms for the neutrinos:

$$M_D = \frac{v}{\sqrt{2}}Y_N \,, \tag{2.8}$$

which mix the left- and right-handed neutrinos. This leads to the full neutrino mass matrix

$$\mathcal{M}_\nu = \begin{pmatrix} 0 & M_D \\ M_D^\intercal & M_R \end{pmatrix}. \tag{2.9}$$

After block diagonalization and in the seesaw limit $||M_D|| \ll ||M_R||$, we obtain the mass eigenvalues for the light neutrinos as

$$m_\nu \simeq -M_D M_R^{-1} M_D^\intercal, \tag{2.10}$$

whereas the RHN mass eigenstates have masses of order M_R. From Eq. (2.10), it is clear that in order to have the correct order of magnitude of light neutrino mass $m_\nu \lesssim 0.1$ eV, as required by oscillation data as well as cosmological constraints, the Yukawa couplings in the canonical seesaw have to be very small, unless the RHNs are super heavy. For instance, for $M_R \sim \mathcal{O}(100 \text{ GeV})$, we require $Y_N \lesssim \mathcal{O}(10^{-6})$. We will see later that these coupling values are too small to have any impact in the RG evolution of other couplings, and thus, the RHNs in the canonical seesaw have effectively no contribution to the vacuum stability in this model.

However, most of the experimental tests of RHNs in the minimal seesaw rely upon larger Yukawa couplings [111, 112]. There are various ways to achieve this theoretically, even for a $\mathcal{O}(100 \text{ GeV})$-scale RHN mass. One possibility is to arrange special textures of M_D and M_R matrices and invoke cancellations among the different elements in Eq. (2.10) to obtain a light neutrino mass [113–120]. Another possibility is the so-called inverse seesaw mechanism [121, 122], where one introduces another set of fermion singlets S_i (with $i = 1, 2, 3$), along with the RHNs N_{R_i}. The corresponding Yukawa Lagrangian is given by

$$\mathcal{L}_{\text{ISS}} = i\overline{N}_R \slashed{\partial} N_R + i\overline{S} \slashed{\partial} S - \left(Y_{N_{ij}} \overline{L}_i \widetilde{\Phi}_1 N_{R_j} + \overline{N}_{R_i} M_{R_{ij}} S_j + \frac{1}{2} \overline{S}_i^c \mu_{S_{ij}} S_j + \text{H.c.} \right), \tag{2.11}$$

where M_R is a 3×3 Dirac mass matrix in the singlet sector and μ_S is the small lepton number breaking mass term for the S-fields. In the basis of $\{\nu_L^c, N_R, S\}$, the full 9×9 neutrino mass matrix takes the form

$$\mathcal{M}_\nu = \begin{pmatrix} 0 & M_D & 0 \\ M_D^\intercal & 0 & M_R \\ 0 & M_R^\intercal & \mu_S \end{pmatrix}. \tag{2.12}$$

After diagonalization of the mass matrix Eq. (2.12) we get the three light neutrino masses

$$m_\nu \simeq M_D M_R^{-1} \mu_S (M_R^\intercal)^{-1} M_D^\intercal, \tag{2.13}$$

whereas the remaining six mass eigenstates are mostly sterile states with masses given by $M_R \pm \mu_S/2$. The key point here is that the presence of additional fermionic singlet and the extra mass term μ_S give us the freedom to accommodate any M_R values while having sizable Yukawa couplings.

Irrespective of the underlying model framework, if we take large $Y_N \sim \mathcal{O}(1)$, it will have a significant negative contribution to the running of quartic couplings via the RHN loop at scales $\mu > M_R$. This must be taken into account in the study of vacuum stability in low-scale seesaw scenarios, as we show below.

3   RG Evolution of the Scalar Quartic Couplings

To study the RG evolution of the couplings, the inert 2HDM+RHN scenario was implemented in `SARAH 4.13.0` [124] and the β-functions for various gauge, quartic and Yukawa couplings in the model are evaluated up to two-loop level. The explicit expressions for the two-loop β-functions can be found in Appendix A, and are used in our numerical analysis of vacuum stability in the next section. To illustrate the effect of the Yukawa and additional scalar quartic couplings on the RG evolution of the SM Higgs quartic coupling λ_1 in the scalar potential (2.3), let us first look at the one-loop β-functions. At the one-loop level, the β-function for the SM Higgs quartic coupling in this model receives three different contributions: one from the SM gauge, Yukawa and quartic interactions, the second from the RHN Yukawa couplings and the third from the inert scalar sector:

$$\beta_{\lambda_1} = \beta_{\lambda_1}^{\text{SM}} + \beta_{\lambda_1}^{\text{RHN}} + \beta_{\lambda_1}^{\text{inert}}, \tag{3.1}$$

with

$$
\begin{aligned}
\beta_{\lambda_1}^{\text{SM}} = \frac{1}{16\pi^2} \Bigg[& \frac{27}{200}g_1^4 + \frac{9}{20}g_1^2 g_2^2 + \frac{9}{8}g_2^4 - \frac{9}{5}g_1^2\lambda_1 - 9g_2^2\lambda_1 + 24\lambda_1^2 \\
& + 12\lambda_1 \text{Tr}\left(Y_u Y_u^\dagger\right) + 12\lambda_1 \text{Tr}\left(Y_d Y_d^\dagger\right) + 4\lambda_1 \text{Tr}\left(Y_e Y_e^\dagger\right) \\
& - 6\text{Tr}\left(Y_u Y_u^\dagger Y_u Y_u^\dagger\right) - 6\text{Tr}\left(Y_d Y_d^\dagger Y_d Y_d^\dagger\right) - 2\text{Tr}\left(Y_e Y_e^\dagger Y_e Y_e^\dagger\right) \Bigg],
\end{aligned} \tag{3.2}
$$

$$\beta_{\lambda_1}^{\text{RHN}} = \frac{1}{16\pi^2}\left[4\lambda_1 \text{Tr}\left(Y_N Y_N^\dagger\right) - 2\text{Tr}\left(Y_N Y_N^\dagger Y_N Y_N^\dagger\right)\right], \tag{3.3}$$

$$\beta_{\lambda_1}^{\text{inert}} = \frac{1}{16\pi^2}\left[2\lambda_3^2 + 2\lambda_3\lambda_4 + \lambda_4^2 + 4\lambda_5^2\right]. \tag{3.4}$$

Here g_1, g_2 are respectively the $U(1)_Y$, $SU(2)_L$ gauge couplings, and Y_u, Y_d, Y_e are respectively the up, down and electron-type Yukawa coupling matrices in the SM. We use the SM input values for these parameters at the EW scale [12]: $\lambda_1 = 0.1264$, $g_1 = 0.3583$, $g_2 = 0.6478$, $y_t = 0.9369$ and other Yukawa couplings are neglected [11].

It is important to note that the RHN contribution to the RG evolution of λ_1 is applicable only above the threshold of M_R.

For illustration, we assume $M_R = 100$ GeV and fix all other quartic coupling values to $\lambda_i = 0.1$ (with $i = 2, 3, 4, 5$) at the EW scale. The added effects of these new contributions in Eq. (3.1) on the RG evolution of the SM Higgs quartic coupling $\lambda_1 \equiv \lambda_h$ as a function of the energy scale μ are shown in Figure 1. Here the red curve shows the RG evolution of λ_h using $\beta_{\lambda_1}^{\rm SM}$ only [cf. Eq. (3.2)], while the blue curve shows the evolution using $\beta_{\lambda_1}^{\rm SM} + \beta_{\lambda_1}^{\rm RHN}$, and finally the green curve shows the full evolution using $\beta_{\lambda_1} \equiv \beta_{\lambda_1}^{\rm SM} + \beta_{\lambda_1}^{\rm RHN} + \beta_{\lambda_1}^{\rm inert}$ [cf. Eq. (3.1)]. The three panels correspond to three benchmark values for the diagonal and degenerate Yukawa coupling values $Y_N = 0.4$ (left), 0.01 (middle), and 10^{-7} (right). As shown in the left panel of Figure 1, for large $Y_N = 0.4$, the negative RHN contribution to the β-function in Eq. (3.3) brings down the stability scale (below which $\lambda_h \geq 0$) from $10^{7.5}$ GeV in the SM (at one-loop level) to 10^7 GeV, which is then neutralized by the positive inert scalar contribution [cf. Eq. (3.4)], that pushes the stability scale back to $10^{8.5}$ GeV and makes $\lambda_h > 0$ again near the Planck scale. As shown in the middle and right panels, for smaller Y_N values, the RHN contribution to the running of λ_h is negligible, and therefore, the red and blue curves almost coincide. In these cases, the addition of inert scalar contribution pushes the stability scale up to 10^{10} GeV, and then λ_h again becomes positive at $\sim 10^{15}$ GeV.

For completeness, we show the full two-loop evolution using the β-functions given in Appendix A in Figure 2. In this case, the stability scale in the SM is $10^{9.5}$ GeV, whereas including the inert scalar contribution always leads to a stable vacuum all the way up to the Planck scale, even for the case when the Yukawa coupling is chosen to be large, $Y_N = 0.4$ (left panel). From this illustration, we conclude that although large Yukawa couplings involving RHNs in low-scale seesaw models tend to destabilize the vacuum at energy scales lower than that in the SM, the additional scalar contributions in the inert 2HDM extension under consideration here have the neutralizing effect of bringing back (or even enhancing) the stability up to higher scales, and in the particular example shown above, all the way up to the Planck scale.

3.1 Stability Bound

The variation of the stability scale with the size of Y_N and λ_i is depicted in Figure 3. For smaller values of λ_i, say 0.1 (red curve), the stability can be ensured up to the Planck scale only for $Y_N \leq 0.30$, beyond which the negative contribution from the RHNs take over and pull λ_h to negative values at scales below the Planck scale. As we increase the λ_i values, the compensating effect from the scalar sector gets enhanced and stability can be ensured up to the Planck scale for higher values of Y_N. This is illustrated by the blue curve corresponding to $\lambda_i = 0.2$, for which $Y_N \leq 0.50$ is allowed. However, arbitrarily increasing λ_i does not help, as the theory encounters
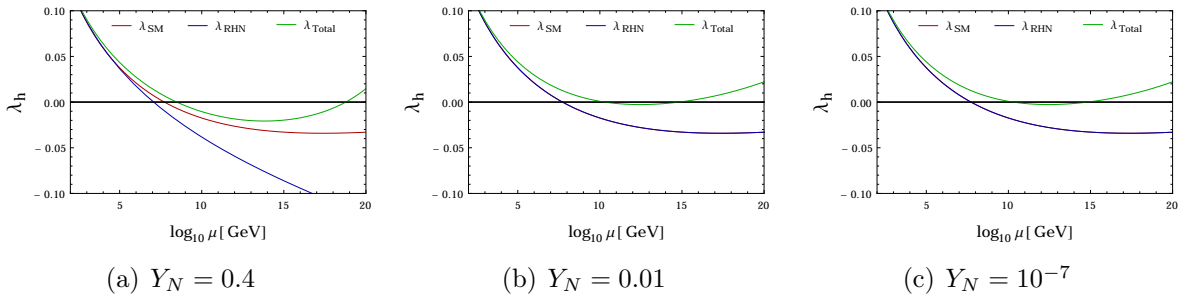
(a) $Y_N = 0.4$ (b) $Y_N = 0.01$ (c) $Y_N = 10^{-7}$

Figure 1. One-loop running of the Higgs quartic coupling λ_h as a function of the energy scale μ for three benchmark values of the Yukawa coupling Y_N. Here we have taken M_R=100 GeV and set $\lambda_{i=2,3,4,5} = 0.1$ for the other quartic couplings at the EW scale. The red, blue, and green curves respectively correspond to the β-functions in the SM, including the RHN contribution and the total contribution including both RHNs and inert scalars to the SM. The horizontal line corresponds to $\lambda_h = 0$, which is the stability line.
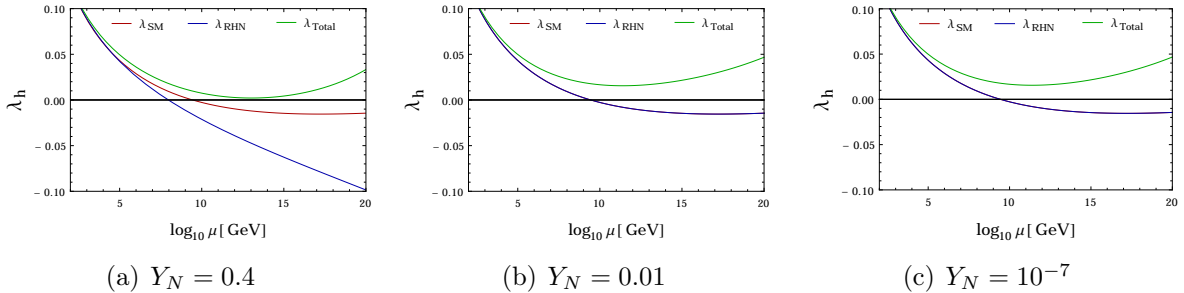

(a) $Y_N = 0.4$ (b) $Y_N = 0.01$ (c) $Y_N = 10^{-7}$

Figure 2. Two-loop running of the Higgs quartic coupling λ_h as a function of energy for three benchmark values of the Yukawa coupling Y_N. Here we have taken M_R=100 GeV and $\lambda_i = 0.1$ for the values of the quartic couplings $\lambda_{2,3,4,5}$ at the EW scale. The red, blue, and green curves respectively correspond to the β-functions in the SM, including the RHN contribution and the total contribution including both RHNs and inert scalars to the SM.

a Landau pole below the Planck scale. For instance, with $\lambda_i = 0.3$ (green curve), a Landau pole is developed at $Y_N = 0.58$ and $\mu = 10^{18.5}$ GeV. Similarly, with $\lambda_i = 0.4$ (purple curve), a Landau pole is developed at $Y_N = 0.55$ and $\mu = 10^{17.8}$ GeV. This leads us to the discussion of the perturbativity bound below.

3.2 Perturbativity Bound

Apart from the stability constraints on the model parameter space, we also need to consider the perturbativity behavior of the dimensionless couplings as we increase the validity scale of the theory. We impose the condition that all dimensionless couplings of the model must remain perturbative for a given value of the energy scale μ, i.e.
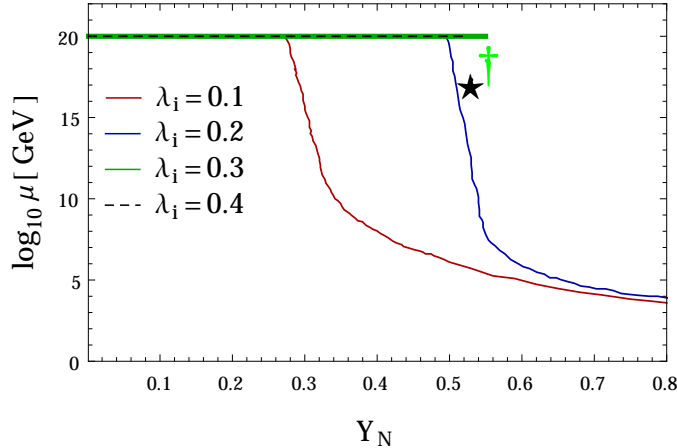
Figure 3. Effect of Yukawa coupling on the stability bound for different values of λ_i. Here, the red curve corresponds to $\lambda_i = 0.10$ which gives stability till the Planck scale for $Y_N \leq 0.30$. The blue curve corresponds to $\lambda_i=0.2$ which gives stability till the Plank scale for $Y_N \leq 0.50$. The green curve corresponds to $\lambda_i=0.3$ which hits Landau pole at $Y_N=0.58$ and $\mu = 10^{18.5}$ GeV. The purple curve corresponds to $\lambda_i=0.4$ which hits Landau pole at $Y_N = 0.55$ and $\mu = 10^{17.8}$ GeV. Otherwise, the green and purple curves almost coincide.

the couplings must satisfy the following constraints:

$$|\lambda_i| \leq 4\pi, \qquad |g_j| \leq 4\pi, \qquad |Y_k| \leq \sqrt{4\pi}, \tag{3.5}$$

where λ_i with $i = 1, 2, 3, 4, 5$ are all scalar quartic couplings, g_j with $j = 1, 2$ are EW gauge couplings,[3] and Y_k with $k = u, d, e, N$ are all Yukawa couplings.

Figure 4 describes the variations of different dimensionless couplings with the energy scale μ. Here we have shown the two-loop RG evolution of g_1 (yellow), g_2 (dotted blue), λ_h (green), λ_3 (red), λ_4 (purple) and λ_5 (blue) as a function of the energy scale μ for benchmark values of $Y_N = 0.53$ and $M_R = 100$ GeV and with the initial conditions g_1=0.3583, g_2=0.6478, λ_h=0.1264, and $\lambda_i = 0.4$ (for $i = 3, 4, 5$) at the EW scale. Three important features are to be noted from this plot: (i) the λ_h coupling becomes non-perturbative at around the scale $\mu \simeq 10^{15}$ GeV, driven by the large Y_N value; (ii) the λ_3 coupling becomes non-perturbative around $10^{8.5}$ GeV until about 10^{16} GeV, again driven by the large Yukawa coupling; and (iii) the gauge couplings g_1 and g_2 hit Landau pole at around the scale $\mu \simeq 10^{17.3}$ GeV. Together, these features imply that the model becomes non-perturbative below the Planck scale for the choice of parameters shown here, in particular for the large Yukawa coupling Y_N chosen in Figure 4. Thus, perturbativity of the couplings up to the Planck scale is an additional constraint we have to take into account along with the vacuum stability constraint.

---

[3]The running of the strong coupling g_3 is same as in the SM, so we do not show it here.
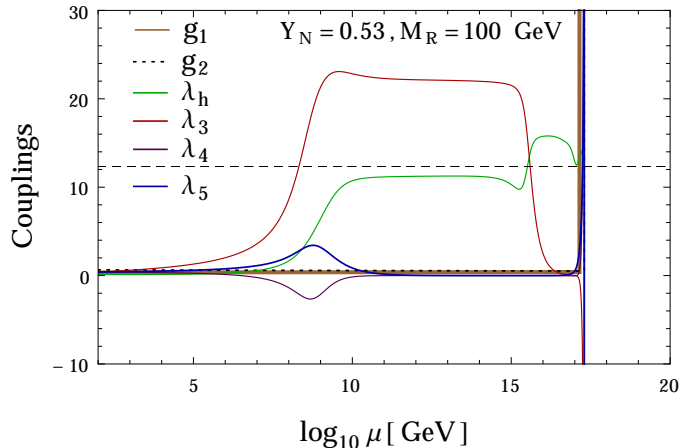
Figure 4. Two-loop RG evolution of dimensionless couplings g_1, g_2, λ_h and λ_i (with $i = 3, 4, 5$) as a function of the energy scale μ for benchmark values of $Y_N = 0.53$, $M_R = 100$ GeV and initial condition for $\lambda_i = 0.4$ at the EW scale. The horizontal dashed line shows the perturbativity limit for scalar quartic and gauge couplings.

The perturbativity behavior of the scalar quartic couplings $\lambda_{3,4,5}$ is studied in Figures 5-7 respectively. In each case, we consider three benchmark values for the Yukawa coupling $Y_N = 0.1$ (left), 0.4 (middle) and 0.9 (right). In each subplot, the various curves correspond to different benchmark initial values for the remaining unknown quartic couplings at the EW scale: red, green, blue and purple respectively for very weak coupling ($\lambda_i = 0.01$), weak coupling ($\lambda_i = 0.1$), moderate coupling ($\lambda_i = 0.4$) and strong coupling ($\lambda_i = 0.8$), while the SM Higgs quartic coupling is fixed at $\lambda_h = 0.126$ and one of the quartic coupling value is varied (as shown along the x-axis) at the EW scale. From Figure 5, we see that for a given Y_N value, the scale at which λ_3 hits the perturbative limit decreases as the scalar effect is increased. For example, in the strong coupling limit (with $\lambda_{2,4,5} = 0.8$ at the EW scale), λ_3 hits the Landau pole at $\mu \sim 10^6$ GeV making the theory non-perturbative much below the Planck scale. As we increase the Y_N value (going from left to right panel), the perturbative limit is reached even for smaller values of λ_i. For instance, for $Y_N = 0.9$ (right panel of Figure 5), λ_3 hits the Landau pole even in the very weak coupling limit (with $\lambda_i = 0.01$) at $\mu \sim 10^{12}$ GeV. The results for λ_4 (cf. Figure 6) and λ_5 (cf. Figure 7) are very similar to those of λ_3 discussed above.

Figure 8 shows the bounds on Yukawa coupling Y_N from perturbativity of λ_i for different initial λ_i values. Here the color coding refers to the size of the Yukawa coupling. For small $Y_N \sim 10^{-7}$ corresponding to the canonical type-I seesaw limit (sky-blue region), no significant effect of RHN is noticed on the perturbativity bound.
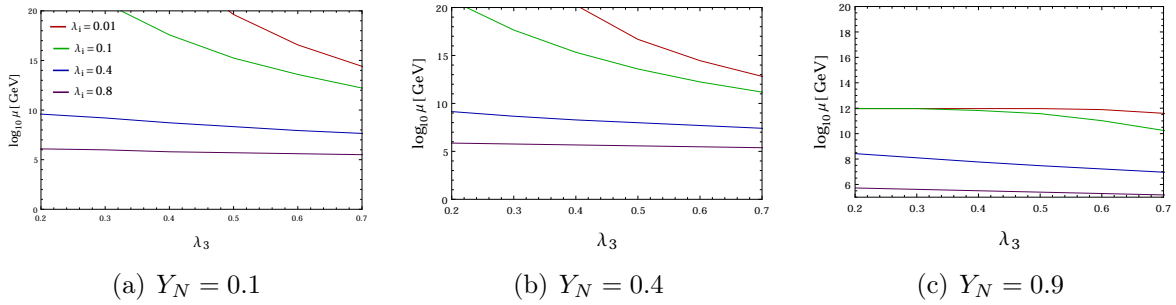
Figure 5. Two-loop running of the scalar quartic coupling λ_3 as a function of energy for three benchmark values of the Yukawa coupling Y_N. Here red, green, blue and purple curves in each plot correspond to different initial conditions for λ_i (with $i = 2, 4, 5$) at the EW scale, representative of very weak ($\lambda_i = 0.01$), weak ($\lambda_i = 0.1$), moderate ($\lambda_i = 0.4$) and strong ($\lambda_i = 0.8$) coupling limits respectively.

Figure 6. Two-loop running of the scalar quartic coupling λ_4 as a function of energy for three benchmark values of the Yukawa coupling Y_N. Here red, green, blue and purple curves in each plot correspond to different initial conditions for λ_i (with $i = 2, 3, 5$) at the EW scale, representative of very weak ($\lambda_i = 0.01$), weak ($\lambda_i = 0.1$), moderate ($\lambda_i = 0.4$) and strong ($\lambda_i = 0.8$) coupling limits respectively.
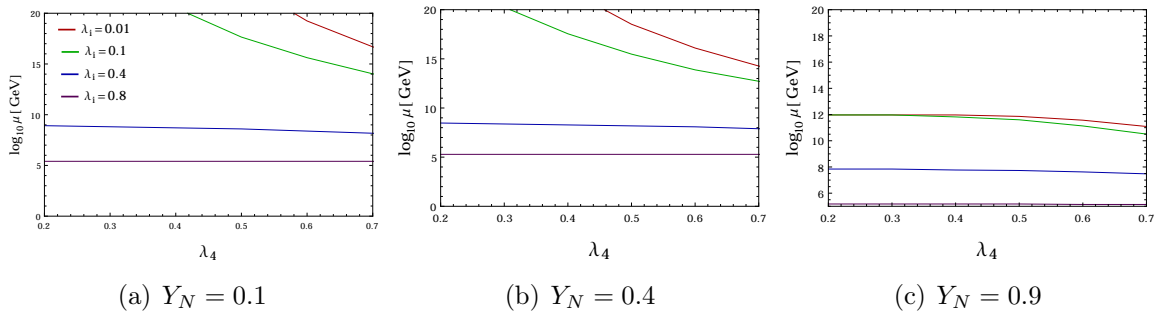
Even if we allow for Y_N values up to 10^{-2} as in low-scale seesaw models with cancellation in the seesaw matrix (yellow region), the effect of RHN on the perturbativity of λ_i is hardly noticeable. However, as we increase Y_N to the level of 0.1 and above, the perturbativity scale decreases quickly due to the negative effect of RHNs in the RG equations. The exact value of Y_N where this starts to happen depends on the initial value of λ_i. For $\lambda_i = 0.1$, the perturbativity scale occurs below the Planck scale and the effect of RHN starts showing up for $Y_N > 0.15$. For $\lambda_i = 0.2$, the perturbativity limit is constant $\sim 10^{16}$ GeV and the effect of RHN starts becoming important for a larger $Y_N > 0.3$ or so. On the other hand, for $\lambda_i = 0.8$, the perturbativity limit is constant at $\sim 10^6$ GeV and the effect of RHN comes much later for $Y_N > 0.8$. Thus as λ_i increases, it can accommodate higher values of Y_N for vacuum stability, but on the contrary, it makes the theory non-perturbative at much lower scale. We infer from Figure 8 that an upper bound comes from perturbativity on λ_i and Y_N
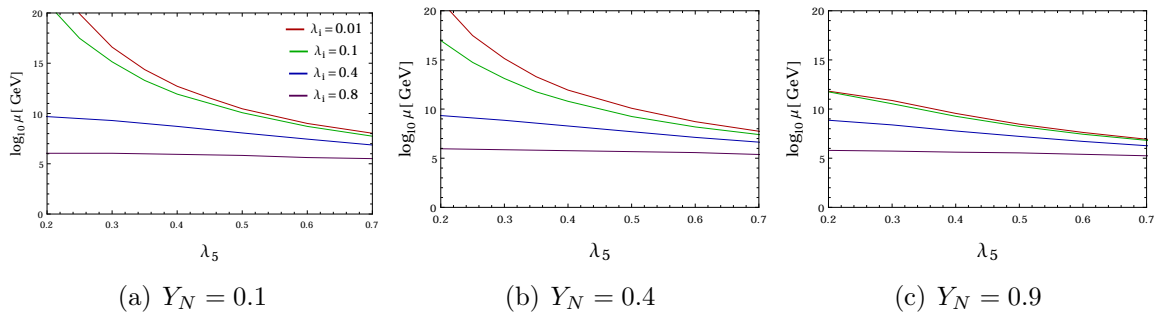
– 11 –

(a) $Y_N = 0.1$ (b) $Y_N = 0.4$ (c) $Y_N = 0.9$

Figure 7. Two-loop running of the scalar quartic coupling λ_5 as a function of energy for three benchmark values of the Yukawa coupling Y_N. Here red, green, blue and purple curves in each plot correspond to different initial conditions for λ_i (with $i = 2, 3, 4$) at the EW scale, representative of very weak ($\lambda_i = 0.01$), weak ($\lambda_i = 0.1$), moderate ($\lambda_i = 0.4$) and strong ($\lambda_i = 0.8$) coupling limits respectively.
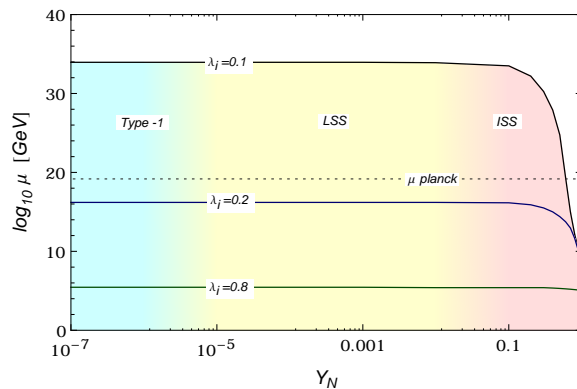

Figure 8. Bounds from perturbativity on Y_N as a function of μ for different values of λ_i with $M_R = 100$ GeV. The color coding refers to the size of Yukawa coupling, with sky-blue, yellow and red-colored regions roughly corresponding to the canonical type-I seesaw, low-scale seesaw (with fine-tuning) and inverse seesaw scenarios.

values, i.e. $\lambda_i \leq 0.15$ and $Y_N \leq 0.3$ for the given theory to remain perturbative till the Planck scale. For comparison, it is worth noting that the perturbativity limit on Y_N derived here is a factor of few weaker than those coming from EW precision data, which vary between 0.02 to 0.07, depending on the lepton flavor, for the minimal seesaw case (i.e. without the inert doublet) [125–129].

4   Vacuum Stability from RG-improved potential

In this section, we investigate the stability of the EW vacuum including the quantum corrections at one-loop level. Here we follow the RG-improved effective potential

approach by Coleman and Weinberg [130], and calculate the effective potential at one-loop for our model. The parameter space of the model is then scanned for the stability, metastability and instability of the potential by calculating the effective Higgs quartic coupling and demanding appropriate limits. We then translate it into constraints on the model parameter space.

The tree-level potential of our inert 2HDM is given in Eq. (2.3). To ensure that the potential is bounded from below in all the directions the tree-level stability conditions are given by [110]

$$\lambda_1 \geq 0, \quad \lambda_2 \geq 0, \quad \lambda_3 \geq -\sqrt{\lambda_1 \lambda_2}, \quad \lambda_3 + \lambda_4 - |\lambda_5| \geq -\sqrt{\lambda_1 \lambda_2}. \qquad (4.1)$$

Considering the running of couplings with the energy scale in the SM, we know that the Higgs quartic coupling λ_h gets a negative contribution from top Yukawa coupling y_t, which makes it negative around 10^{10-11} GeV and we expect a second deeper minimum for the high field values. Since the other minimum exists at much higher scale than the EW minimum, we can safely consider the effective potential in the h-direction to be

$$V_{\text{eff}}(h, \mu) \simeq \lambda_{\text{eff}}(h, \mu) \frac{h^4}{4}, \quad \text{with } h \gg v, \qquad (4.2)$$

where $\lambda_{\text{eff}}(h, \mu)$ is the effective quartic coupling which can be calculated from the RG-improved potential. The stability of the vacuum can then be guaranteed at a given scale μ by demanding that $\lambda_{\text{eff}}(h, \mu) \geq 0$. We follow the same strategy as in the SM in order to calculate $\lambda_{\text{eff}}(h, \mu)$ in our model, as described below.

4.1 Effective Potential

The one-loop RG-improved effective potential in our model can be written as

$$V_{\text{eff}} = V_0 + V_1^{\text{SM}} + V_1^{\text{inert}} + V_1^{\text{RHN}}, \qquad (4.3)$$

where V_0 is the tree-level potential given by Eq. (2.3), V_1^{SM} is the effective Coleman-Weinberg potential in the SM that contains all the one-loop corrections involving the SM particles at zero temperature with vanishing momenta, V_1^{inert} and V_1^{RHN} are the corresponding one-loop effective potential terms from the inert scalar doublet and the RHN loops in the model. In general, V_1 can be written as

$$V_1(h, \mu) = \frac{1}{64\pi^2} \sum_i (-1)^F n_i M_i^4(h) \left[\log \frac{M_i^2(h)}{\mu^2} - c_i \right], \qquad (4.4)$$

where the sum runs over all the particles that couple to the h-field, $F = 1$ for fermions in the loop and 0 for bosons, n_i is the number of degrees of freedom of each particle, M_i^2 are the tree-level field-dependent masses given by

$$M_i^2(h) = \kappa_i h^2 - \kappa_i', \qquad (4.5)$$

with the coefficients given in Table 1. In the last column, m^2 corresponds to the tree-level Higgs mass parameter. Note that the massless particles do not contribute to Eq. (4.5), and hence, neither to Eq. (4.4). Therefore, for the SM fermions, we only include the dominant contribution from top quarks, and neglect the other quarks. It is also important to note that the RHN contributions come after each threshold value of M_{R_i}.

Particles	i	F	n_i	c_i	κ_i	κ'_i
	$W^\pm$	0	6	5/6	$g_2^2/4$	0
	Z	0	3	5/6	$(g_1^2 + g_2^2)/4$	0
SM	t	1	12	3/2	Y_t^2	0
	h	0	1	3/2	λ_h	m^2
	$G^\pm$	0	2	3/2	λ_h	m^2
	G^0	0	1	3/2	λ_h	m^2
	$H^\pm$	0	2	3/2	$\lambda_3/2$	0
Inert	H	0	1	3/2	$(\lambda_3 + \lambda_4 + 2\lambda_5)/2$	0
	A	0	1	3/2	$(\lambda_3 + \lambda_4 - 2\lambda_5)/2$	0
RHN	N_i	1	2	3/2	$Y_N^2/2$	0

Table 1. Coefficients entering in the Coleman-Weinberg effective potential, cf. Eq. (4.4).

Using Eq. (4.4) for the one-loop potentials, the full effective potential in Eq. (4.3) can be written in terms of an effective quartic coupling as in Eq. (4.2). This effective coupling can be written as follows:

$$
\lambda_{\text{eff}}(h, \mu) \simeq \underbrace{\lambda_h(\mu)}_{\text{tree-level}} + \frac{1}{16\pi^2} \Bigg\{ \underbrace{\sum_{\substack{i=W^\pm, Z, t, \\ h, G^\pm, G^0}} n_i \kappa_i^2 \Big[\log \frac{\kappa_i h^2}{\mu^2} - c_i \Big]}_{\text{Contribution from SM}}
$$

$$
+ \underbrace{\sum_{i=H, A, H^\pm} n_i \kappa_i^2 \Big[\log \frac{\kappa_i h^2}{\mu^2} - c_i \Big]}_{\text{Contribution from inert doublet}} + 2 \underbrace{\sum_{i=1,2,3} n_i \kappa_i^2 \Big[\log \frac{\kappa_i h^2}{\mu^2} - c_i \Big]}_{\text{Contribution from RHN}} \Bigg\}. \quad (4.6)
$$

Note that in the inverse seesaw case and in the limit $\mu_S \to 0$, each of the RHN mass eigenvalue is double-degenerate, and therefore, we have an extra factor of two for each RHN contribution in Eq. (4.6). The nature of $\lambda_{\text{eff}}(h, \mu)$ in our model thus guides us to identify the possible instability and metastability regions, as discussed below. We take the field value $h = \mu$ for the numerical analysis as at that scale the potential remains scale-invariant [131].

4.2 Stable, Metastable and Unstable Regions

The parameter space where $\lambda_{\text{eff}} \geq 0$ is termed as the *stable* region, since the EW vacuum is the global minimum in this region. For $\lambda_{\text{eff}} < 0$, there exists a second minimum deeper than the EW vacuum. In this case, the EW vacuum could be either unstable or metastable, depending on the tunneling probability from the EW vacuum to the true vacuum. The parameter space with $\lambda_{\text{eff}} < 0$, but with the tunneling lifetime longer than the age of the universe is termed as the *metastable* region. The expression for the tunneling probability to the deeper vacuum at zero temperature is given by

$$P \;=\; T_0^4 \mu^4 \exp\left[\frac{-8\pi^2}{3\lambda_{\text{eff}}(\mu)}\right] , \tag{4.7}$$

where T_0 is the age of the universe and μ denotes the scale where the probability is maximized, i.e. $\frac{\partial P}{\partial \mu} = 0$. This gives us a relation between the λ values at different scales:

$$\lambda_{\text{eff}}(\mu) \;=\; \frac{\lambda_{\text{eff}}(v)}{1 - \frac{3}{2\pi^2} \log\left(\frac{v}{\mu}\right) \lambda_{\text{eff}}(v)} , \tag{4.8}$$

where $v \simeq 246$ GeV is the EW VEV. Setting $P = 1$, $T = 10^{10}$ years and $\mu = v$ in Eq. (4.7), we find $\lambda_{\text{eff}}(v) = 0.0623$. The condition $P < 1$, for a universe about $T = 10^{10}$ years old is equivalent to the requirement that the tunneling lifetime from the EW vacuum to the deeper one is larger than T_0 and we obtain the following condition for metastability [8]:

$$0 \;>\; \lambda_{\text{eff}}(\mu) \;\gtrsim\; \frac{-0.065}{1 - 0.01 \log\left(\frac{v}{\mu}\right)} . \tag{4.9}$$

The remaining parameter space with $\lambda_{\text{eff}} < 0$, where the condition (4.9) is not satisfied is termed as the *unstable* region. As can be seen from Eq. (4.6), these regions depend on the energy scale μ, as well as the model parameters, including the RHN mass and the gauge, scalar quartic and Yukawa couplings (see also Ref. [132]).

Figure 9 shows the variation of λ_{eff} in our model with the energy scale for different values of λ_i (with $i = 2, 3, 4, 5$) and M_R values with a fixed $Y_N = 0.4$. The three different lines correspond to different values of the top Yukawa coupling by varying the top mass from 170 to 176 GeV with median value at 173 GeV [10]. The red region in Figure 9 corresponds to the instability region and the yellow region below the horizontal line $\lambda_{\text{eff}} = 0$ corresponds to the metastable region, whereas the green region above $\lambda_{\text{eff}} = 0$ is the stability region. Figure 9(a) and Figure 9(b) show that as the values of λ_i are increased from 0.01 to 0.1 for the same value of $Y_N = 0.4$ and $M_R = 10^3$, λ_{eff} becomes unstable at 10^{15} GeV instead of 10^{11} GeV (with higher end of

(a) $\lambda_i = 0.01$, $M_R = 10^3$ GeV

(b) $\lambda_i = 0.1$, $M_R = 10^3$ GeV

(c) $\lambda_i = 0.01$, $M_R = 10^4$ GeV

(d) $\lambda_i = 0.1$, $M_R = 10^4$ GeV

(e) $\lambda_i = 0.01$, $M_R = 10^8$ GeV

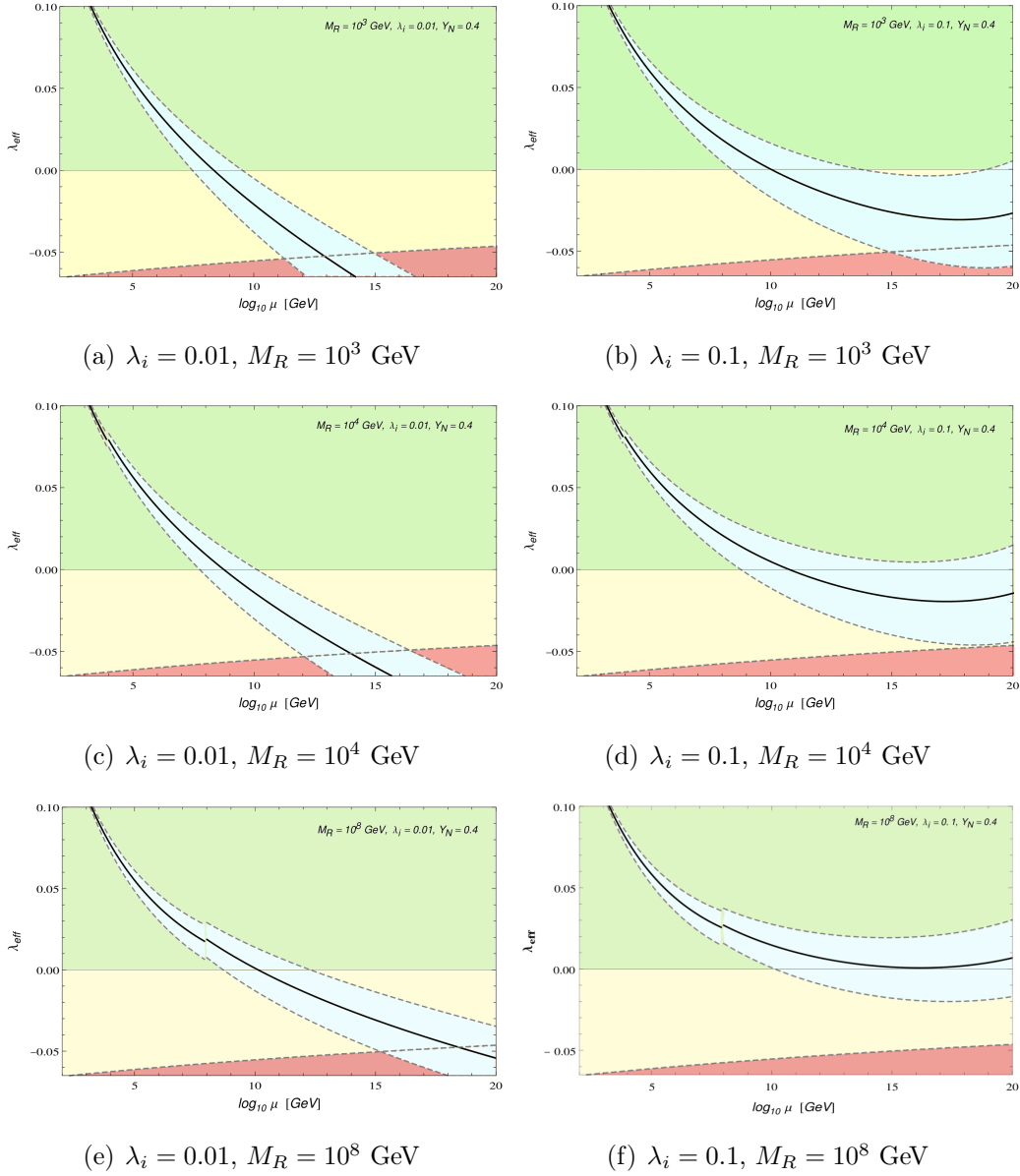(f) $\lambda_i = 0.1$, $M_R = 10^8$ GeV

Figure 9. Running of λ_{eff} with energy scale for six different scenarios: $\lambda_i = 0.01$ (left) and 0.1 (right); $M_R = 10^3$ GeV (top), 10^4 GeV (middle) and 10^8 GeV (bottom). We have fixed $Y_N = 0.4$ in all the subplots. The three different lines for λ_{eff} correspond to different values of the top Yukawa coupling obtained by varying the top mass from 170 GeV (upper dashed line) to 176 GeV (lower dashed line) with the median value of 173 GeV (middle solid line). The red, yellow and green regions correspond to the unstable, metastable and stable regions, respectively.

the top mass). Figure 9(a), Figure 9(c) and Figure 9(e) [or Figure 9(b), Figure 9(d) and Figure 9(f)] show that for fixed λ_i and Y_N, the stability scale also gets enhanced as we increase RHN mass M_R, because the RHNs contribute to the β-function only at scales $\mu \geq M_R$. This is the reason for the discontinuity at M_R value, which is
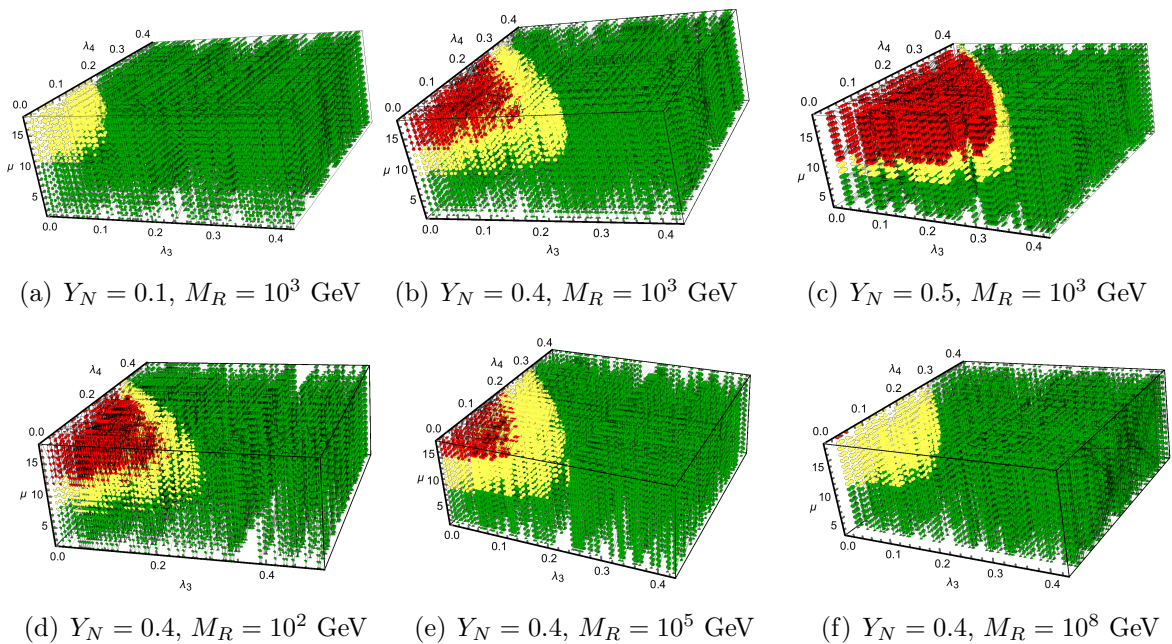
Figure 10. Three-dimensional correlation plot for λ_3 versus λ_4 with energy scale [log(10) in GeV] in six different scenarios. In the top three panels, we fix $M_R = 10^3$ GeV, $y_t = 0.93693$ and vary Y_N from 0.1 (left) to 0.4 (middle) and 0.5 (right). In the bottom three panels, we fix $Y_N = 0.4$ and vary M_R from 10^2 GeV (left) to 10^5 GeV (middle) and 10^8 GeV (right). In all the subplots, we have fixed $\lambda_2 = \lambda_5 = 0.01$. The red, yellow and green regions correspond to the unstable, metastable and stable regions, respectively.

obvious in Figure 9(e) and Figure 9(f).

To see the individual effects of the scalar quartic couplings $\lambda_{2,3,4,5}$ on the stability scale, we show in Figure 10 the three-dimensional correlation plots for λ_3 versus λ_4 with energy scale μ for different values of Y_N and M_R with a fixed $\lambda_2 = \lambda_5 = 0.01$. As in Figure 9, the red, yellow and green regions correspond to the unstable, metastable and stable regions respectively. Figure 10(a), Figure 10(b) and Figure 10(c) show the effect of the RHN Yukawa coupling on the stability scale. For smaller Y_N =0.1, there is no unstable region. As the value of Y_N is increased to 0.4 and 0.5 the stability and metastability regions decrease, while the unstable region increases. Similarly, Figure 10(d). Figure 10(e) and Figure 10(f) describe the dependence on the M_R scale. Here the metastable and stable regions increase as we increase the value of M_R from 10^2 to 10^8 GeV.

As can be seen from Figure 9, the stability scale crucially depends on the top Yukawa coupling. The running of $\lambda_{\rm eff}$ also depends on the initial value of λ_h, which comes from the experimental value of the SM Higgs mass. Figure 11 shows the stability phase diagram in terms of Higgs boson mass and top pole mass for two different choices of $Y_N = 10^{-7}$ and 0.38 while keeping M_R fixed at 100 GeV. The
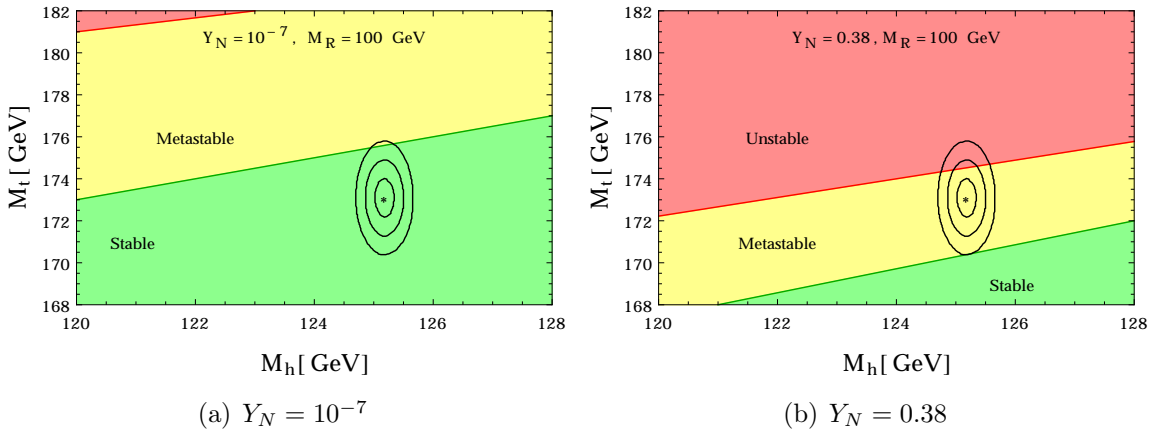
Figure 11. Stability phase diagram in terms of the SM Higgs boson and top-quark pole masses. Here we have fixed $\lambda_i = 0.1$ and $M_R = 100$ GeV, while Y_N is varied from 10^{-7} (left) to $Y_N = 0.38$ (right). The red, yellow and green regions correspond to the unstable, metastable and stable regions respectively, which change depending on the model parameters. The contours and the dot show the current experimental $1\sigma, 2\sigma, 3\sigma$ regions and central value in the (M_h, M_t) plane.

contours show the current experimental $1\sigma, 2\sigma, 3\sigma$ regions in the (M_h, M_t) plane, while the dot represents the central value [12]. Figure 11(a) describes that for small $Y_N = 10^{-7}$, the current 3σ values for the Higgs boson mass and top mass mostly lie in the stable region. However, as Y_N is increased to a large value of 0.38 in Figure 11(b), the Higgs boson mass value lies in the stable region but the top mass value lies in the unstable/metastable region. The bound that comes on Y_N from stability for which both Higgs boson mass and the top mass lie in the stability region is $Y_N \lesssim 0.32$ for $M_R = 100$ GeV and $\lambda_i = 0.1$.

5 LHC Phenomenology

The collider phenomenology of inter Higgs doublet with RHN is quite interesting as some decay modes involving RHNs are not allowed due to the Z_2 symmetry and this feature can be used to distinguish it from other scenarios. The pseudoscalar boson, the heavy CP-even Higgs boson and the charged Higgs boson $(A, H, H^{\pm})$ are all from the inert doublet Φ_2, which is Z_2 odd and their mass splittings are mostly $\lesssim M_W$ [cf. Eq. (2.6)]. However, mass splittings around $\gtrsim M_{W^{\pm},Z}$ are also possible some parameter space. The Z_2 symmetry prohibits any kind of mass-mixing of these inert Higgs bosons with the SM-like Higgs boson, which is coming from Z_2-even Φ_1. The couplings of Φ_2 with fermions are also prohibited, leaving only the gauge and scalar couplings. Nevertheless, as shown above, the inert Higgs doublet Φ_2 plays a crucial role in determining the stability and perturbativity conditions, and therefore, it is important to study their potential signatures at colliders. In Table 2 we present

BP	λ_3	λ_4	λ_5	m_{22}	M_H	M_A	$M_{H^\pm}$
BP1	0.10	0.10	0.10	200	228.26	200.00	207.42
BP2	0.10	0.10	0.10	300	319.53	300.00	305.00
BP3	0.20	0.20	0.20	250	294.53	250.00	261.84
BP4	0.11	0.11	-0.20	200	185.88	242.40	208.15
BP5	0.22	0.22	-0.16	300	305.99	336.14	310.89
BP6	0.32	-0.10	-0.01	300	309.92	311.86	315.72
BP7	0.32	-0.20	-0.08	250	247.56	266.40	268.66
BP8	0.29	0.31	0.31	2200	2208.38	2199.86	2201.99
BP9	0.23	0.11	0.12	1200	1207.30	1201.26	1202.90
BP10	0.20	0.23	0.28	2000	2007.48	1999.01	2001.51

Table 2. Benchmark points allowed by the vacuum stability, perturbativity and DM constraints. Here we have chosen $Y_N = 0.4$ and $M_R = 1$ TeV.

Decay Modes	BR in percentage
$N_i \to h W^\pm \ell^\mp$	0.36
$N_i \to H H^\pm \ell^\mp$	2.4×10^{-4}
$N_i \to A H^\pm \ell^\mp$	5.2×10^{-5}

Table 3. Dominant three-body decay BRs of RHN involving Higgs bosons in the final states for a benchmark point allowed by the vacuum stability and perturbativity with $M_R = 1$ TeV. Note that these BRs are independent of the choice of Y_N.

ten benchmark points for the future collider study which are allowed by the vacuum stability and perturbativity bounds. The scenario with the lightest charged Higgs bosons ($H^\pm$) causes an electromagnetically-charged DM candidate and such points are phenomenologically disallowed. This leaves us with two kind of scenarios with either H or A as the lightest heavy scalar, to be identified as the DM candidate.

The RHNs on the other hand only couple to Φ_1, leaving the Yukawa interactions with the SM-like Higgs boson. Via their mixing with the light neutrinos, the RHNs also couple to the SM W and Z gauge bosons after EW symmetry breaking, which
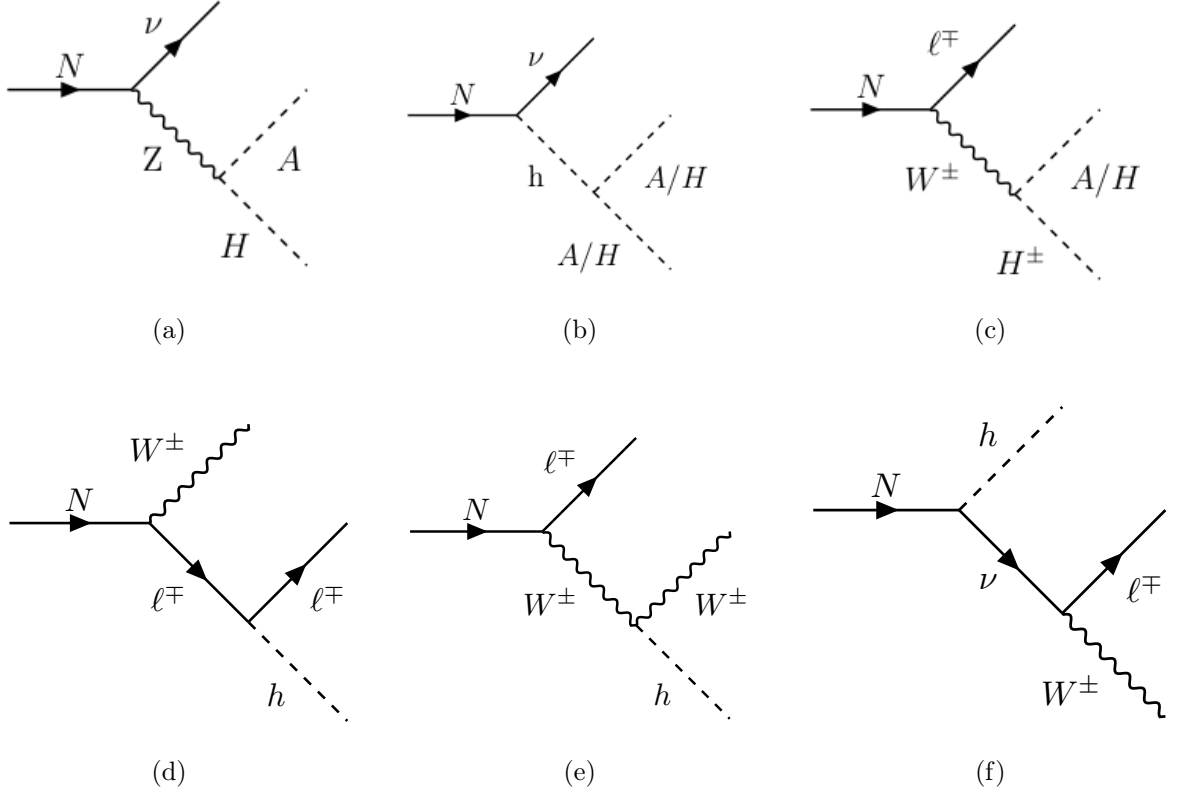
Figure 12. Various three-body decays of RHNs involving heavy Higgs bosons in the final state: (a) Decay to light neutrinos and H/A via an off-shell Z boson; (b) decay to light neutrinos and H/A pairs via an off-shell Higgs boson; (c) decay to a charged-lepton and charged Higgs boson in association with H/A via an off-shell W boson; (d)-(f) decay to a charged lepton and SM W and Higgs bosons.

are proportional to the VEV of Φ_1 and decay dominantly to $W^\pm \ell^\mp$, $Z\nu$, and $h\nu$. In principle, the RHN sector and the inert scalar sector do not talk to each other. However, couplings with the gauge sectors open up a window to the inert Higgs sector from the RHN decay. This is possible via the three-body decays of the RHNs with heavy Higgs bosons in the final states that can be seen from Figure 12. The RHNs can decay to light neutrinos and H, A via an off-shell Z boson [cf. Figure 12(a)], to light neutrinos and H/A pairs via a off-shell h [cf. Figure 12(b)], to a charge lepton and charged Higgs boson in association with H/A [cf. Figure 12(c)], and to a charged lepton and SM Higgs boson in association with $W^\pm$ [cf. Figures 12(d)-12(f)]. For a RHN with mass 1 TeV, though the two-body decay modes (with on-shell $W^\pm, Z$ and h) dominate, but the three-body decay modes involving the heavy Higgs sector can still be explored at the LHC. The highest three-body decay mode is $N_i \to hW^\pm \ell^\mp$ [cf. Figure 12(d)] with branching ratio (BR) $\sim 0.36\%$ and other modes

Parameters		$\sigma(gg \rightarrow \sum_i N_i\nu_i)$ in fb		$\sigma(gg \rightarrow \sum_i N_iN_i)$ in fb		$\sigma_{DY}(pp \rightarrow \sum_i N_i + X)$ in fb	
Y_N	M_R in GeV	14 TeV	100 TeV	14 TeV	100 TeV	14 TeV	100 TeV
0.1	500	0.15	9.70	1.8×10^{-4}	1.2×10^{-2}	0.34	6.90
0.1	1000	1.6×10^{-3}	0.36	5.0×10^{-7}	1.1×10^{-4}	4.5×10^{-3}	0.18
0.4	500	2.40	155.40	0.30	0.50	5.00	95.60
0.4	1000	0.03	5.83	1.2×10^{-4}	0.03	0.06	2.55

Table 4. NLO production cross-sections of the RHNs at the LHC for 14 TeV and 100 TeV center of mass energy. Here the other parameters are as in BP3 of Table 2.

are with $BR(N_i \rightarrow HH^{\pm}\ell^{\mp}) \sim 2.4 \times 10^{-4}\%$ and $BR(N_i \rightarrow AH^{\pm}\ell^{\mp}) \sim 5.2 \times 10^{-5}\%$ respectively, as given in Table 3 for $Y_N = 0.01$ and $M_R = 1$ TeV.
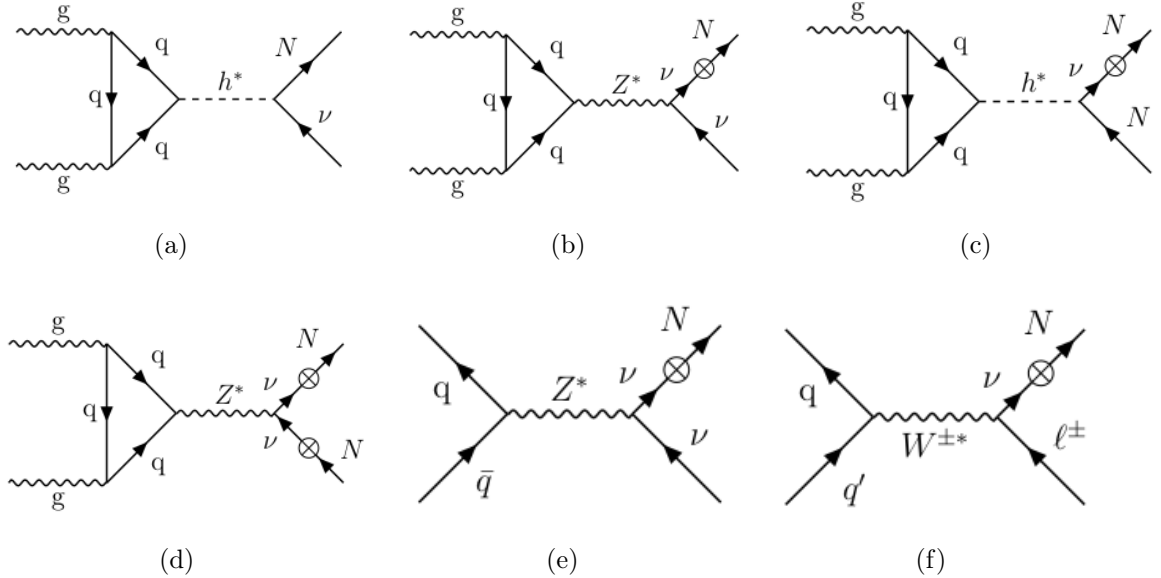
Figure 13. Feynman diagrams for RHN production via either gluon-gluon fusion [(a) to (d)] or Drell-Yan process [(e) and (f)]. The cross $\otimes$ indicates light-heavy neutrino mixing.

As for the RHN production at the LHC, being SM gauge-singlets, they can only be produced via their mixing with active neutrinos in the minimal seesaw model. The dominant production modes are shown in Figure 13. There are two types of processes: (a)-(d) involve RHN production via off-shell Higgs boson from gluon-gluon fusion,

whereas (e)-(f) involve production via off-shell $W^{\pm}/Z$ from Drell-Yan processes. The next-to-leading order (NLO) cross-sections for $Y_N = 0.1, 0.4$ and $M_R = 500$ GeV, 1 TeV are given in Table 4 where other parameters are kept as in BP3 of Table 2. For the process $N\nu$ [cf. Figure 13(a)], the production cross-section at NLO for $Y_N = 0.1$ and $M_R = 500$ GeV is: $\sigma(gg \rightarrow \sum_{i=1,2,3} N_i\nu_i)$ is ~ 0.15 and 9.7 fb respectively at the LHC with 14 TeV and 100 TeV center of mass energy [133]. For pair production the cross-sections are 1.8×10^{-4} and 1.2×10^{-3} respectively at the LHC with 14 TeV and 100 TeV center of mass energy. Here we have used `CalcHEP 3.7.5` [134] for calculating the tree-level cross sections and decay branching fraction and have chosen `NNPDF 3.0 QED NLO` [135] and $\sqrt{\hat{s}}$ (parton-level center of mass energy) as the energy scale for the cross-section calculations. The third column of Table 4 also give NLO Drell-Yan cross-sections for the same scale and PDF. We can see that for $\sqrt{s} = 14$ TeV at the LHC Drell-Yan processes are more dominant than gluon gluon fusion, whereas at $\sqrt{s} = 100$ TeV gluon gluon fusion processes surpass Drell-Yan ones. Though the overall cross-sections are small, but higher luminosity LHC can probe these three-body decays. The maximum cross-section comes for $Y_N = 0.4$ and $M_R = 500$ GeV and for $\sqrt{s} = 100$ TeV and these are 155.40 fb, 95.60 fb, 0.50 fb respectively for $(gg \rightarrow \sum_i N_i\nu_i)$, $(pp \rightarrow \sum_i N_i + X)_{\rm DY}$ and $(gg \rightarrow \sum_i N_iN_i)$. Note that although such large values of Y_N might have been excluded from indirect constraints such as EW precision data, it is still useful to get an independent direct constraint from the collider searches.

Coming to the inert Higgs boson signatures we have to rely on the mass spectrum of the Higgs bosons which depend on the couplings $\lambda_{3,4,5}$ as shown in Eq. (2.6). Table 2 shows benchmark points with the $\lambda_{3,4,5}$ that are allowed by the vacuum stability and perturbativity conditions. Depending on the phase space available, the charged Higgs boson in this model can decay into $AW^{\pm}$ and/or $HW^{\pm}$ mostly via off-shell W boson as the heavy Higgs bosons stay degenerate. The lighter of A and H is the DM candidate and thus can give rise to the signature of mono-lepton plus missing energy or dijet plus missing energy. However, because of the Z_2-odd nature of $H, A, H^{\pm}$ we can only produce the charged Higgs bosons as pair or in association with H/A. The heavier of A/H in that case decays to dilepton plus missing energy via off-shell Z boson. The production of $H^{\pm}$ pair gives rise to dilepton plus missing energy and $H^{\pm}A/H$ give rise to trilepton or mono-lepton plus missing energy signatures, which can be searched for at the LHC and FCC-hh [136]. The inert Higgs boson productions in association with the DM candidate leaving to jet plus lepton and missing energy signatures are studied in Ref. [137]. The inert doublet signatures along with the three-body decays of RHNs with Higgs boson in the final state can shed light on this model at the LHC with higher luminosity.

The LHC phenomenology discussed here is different from $U(1)'$ extensions where the RHNs can be pair-produced at the LHC via the $U(1)'$ gauge boson [138–142]. Phenomenological signatures of such RHN decays in the type-I seesaw in presence of

extra scalars have been studied in the literature [143–147]. Similarly, in the case of type-III seesaw, the RHNs have charged partner and couple to $W^{\pm}$ bosons [148]. The LHC phenomenology of such extensions with and without additional Higgs doublet has also been looked into [149–151]. The inverse-seesaw phenomenologies probing the RHNs at the LHC along with heavier Higgs bosons were also examined [152, 153].

6   Conclusion

We have considered a simple extension of the SM with a Z_2-odd inert Higgs doublet, supplemented by right-handed neutrinos with potentially large Dirac Yukawa couplings. The neutral part of the inert-Higgs doublet is a suitable DM candidate, while the RHNs are responsible for the correct light neutrino masses via seesaw mechanism. We have studied the effect of these new scalars and fermions on the stability of the EW vacuum by performing an RG analysis for the scalar quartic couplings.

We find that the additional scalars enhance the EW stability bound with respect to the SM case, as expected. Although the introduction of RHNs with relatively larger Yukawa couplings can be a spoiler for vacuum stability, the inert doublet comes to a rescue by contributing positively to the β-functions. On the other hand, the scalar quartic couplings cannot take arbitrarily large values at the EW scale due to perturbativity considerations at higher scales. In particular, we find upper bounds on the scalar quartic couplings λ_i (with $i = 2, 3, 4, 5$) and the Dirac Yukawa couplings Y_N, depending on the RHN mass scale M_R, to satisfy both stability and perturbativity constraints.

We also analyzed the RG-improved effective potential to identify the regions of parameter space giving rise to stable, metastable and unstable vacua. For fixed values of λ_i, increasing Y_N enlarges the unstable vacuum region, whereas decreasing Y_N and/or increasing the RHN mass scale M_R enhances the stability prospects.

We also studied the phenomenological signatures of the heavy Higgs bosons along with RHNs at the LHC and future 100 TeV collider. Since the heavy Higgs bosons in this model come from the Z_2-odd doublet, they are relatively non-interacting with the SM particles and are almost mass-degenerate, thus making their collider searches rather difficult. We have identified some new three-body decay modes of the RHNs to heavy Higgs bosons (assuming that the RHNs are heavier than the Higgs bosons) which can be used to distinguish this model from other vanilla RHN models.

Acknowledgments

A   Two-loop β-functions

A.1   Scalar Quartic Couplings

$$
\begin{aligned}
\beta_{\lambda_1} ={}& \frac{1}{16\pi^2}\Bigg[\frac{27}{200}g_1^4 + \frac{9}{20}g_1^2 g_2^2 + \frac{9}{8}g_2^4 - \frac{9}{5}g_1^2\lambda_1 - 9g_2^2\lambda_1 + 24\lambda_1^2 + 2\lambda_3^2 + 2\lambda_3\lambda_4 + \lambda_4^2 + 4\lambda_5^2 \\
& + 12\lambda_1\mathrm{Tr}\left(Y_d Y_d^\dagger\right) + 4\lambda_1\mathrm{Tr}\left(Y_e Y_e^\dagger\right) + 4\lambda_1\mathrm{Tr}\left(Y_N Y_N^\dagger\right) + 12\lambda_1\mathrm{Tr}\left(Y_u Y_u^\dagger\right) \\
& - 6\mathrm{Tr}\left(Y_d Y_d^\dagger Y_d Y_d^\dagger\right) - 2\mathrm{Tr}\left(Y_e Y_e^\dagger Y_e Y_e^\dagger\right) - 6\mathrm{Tr}\left(Y_u Y_u^\dagger Y_u Y_u^\dagger\right) - 2\mathrm{Tr}\left(Y_N Y_N^\dagger Y_N Y_N^\dagger\right)\Bigg] \\
& + \frac{1}{(16\pi^2)^2}\Bigg[-\frac{3537}{2000}g_1^6 - \frac{1719}{400}g_1^4 g_2^2 - \frac{303}{80}g_1^2 g_2^4 + \frac{291}{16}g_2^6 + \frac{1953}{200}g_1^4\lambda_1 + \frac{117}{20}g_1^2 g_2^2\lambda_1 \\
& - \frac{51}{8}g_2^4\lambda_1 + \frac{108}{5}g_1^2\lambda_1^2 + 108g_2^2\lambda_1^2 - 312\lambda_1^3 + \frac{9}{10}g_1^4\lambda_3 + \frac{15}{2}g_2^4\lambda_3 + \frac{12}{5}g_1^2\lambda_3^2 + 12g_2^2\lambda_3^2 \\
& - 20\lambda_1\lambda_3^2 - 8\lambda_3^3 + \frac{9}{20}g_1^4\lambda_4 - \frac{3}{2}g_1^2 g_2^2\lambda_4 + \frac{15}{4}g_2^4\lambda_4 + \frac{12}{5}g_1^2\lambda_3\lambda_4 + 12g_2^2\lambda_3\lambda_4 \\
& - 20\lambda_1\lambda_3\lambda_4 - 12\lambda_3^2\lambda_4 + \frac{6}{5}g_1^2\lambda_4^2 + 3g_2^2\lambda_4^2 - 12\lambda_1\lambda_4^2 - 16\lambda_3\lambda_4^2 - 6\lambda_4^3 - \frac{12}{5}g_1^2\lambda_5^2 \\
& - 56\lambda_1\lambda_5^2 - 80\lambda_3\lambda_5^2 + 8\lambda_4\lambda_5^2 + \frac{1}{20}\Big(-5\big(64\lambda_1\big(-5g_3^2 + 9\lambda_1\big) - 90g_2^2\lambda_1 + 9g_2^4\big) \\
& + 9g_1^4 + g_1^2\big(50\lambda_1 + 54g_2^2\big)\Big)\mathrm{Tr}\left(Y_d Y_d^\dagger\right) - \frac{3}{20}\Big(15g_1^4 - 2g_1^2\big(11g_2^2 + 25\lambda_1\big) \\
& + 5\big(-10g_2^2\lambda_1 + 64\lambda_1^2 + g_2^4\big)\Big)\mathrm{Tr}\left(Y_e Y_e^\dagger\right) - \frac{9}{100}g_1^4\mathrm{Tr}\left(Y_N Y_N^\dagger\right) \\
& - \frac{3}{10}g_1^2 g_2^2\mathrm{Tr}\left(Y_N Y_N^\dagger\right) - \frac{3}{4}g_2^4\mathrm{Tr}\left(Y_N Y_N^\dagger\right) + \frac{3}{2}g_1^2\lambda_1\mathrm{Tr}\left(Y_N Y_N^\dagger\right) + \frac{15}{2}g_2^2\lambda_1\mathrm{Tr}\left(Y_N Y_N^\dagger\right) \\
& - 48\lambda_1^2\mathrm{Tr}\left(Y_N Y_N^\dagger\right) - \frac{171}{100}g_1^4\mathrm{Tr}\left(Y_u Y_u^\dagger\right) + \frac{63}{10}g_1^2 g_2^2\mathrm{Tr}\left(Y_u Y_u^\dagger\right) - \frac{9}{4}g_2^4\mathrm{Tr}\left(Y_u Y_u^\dagger\right) \\
& + \frac{17}{2}g_1^2\lambda_1\mathrm{Tr}\left(Y_u Y_u^\dagger\right) + \frac{45}{2}g_2^2\lambda_1\mathrm{Tr}\left(Y_u Y_u^\dagger\right) + 80g_3^2\lambda_1\mathrm{Tr}\left(Y_u Y_u^\dagger\right) - 144\lambda_1^2\mathrm{Tr}\left(Y_u Y_u^\dagger\right) \\
& + \frac{4}{5}g_1^2\mathrm{Tr}\left(Y_d Y_d^\dagger Y_d Y_d^\dagger\right) - 32g_3^2\mathrm{Tr}\left(Y_d Y_d^\dagger Y_d Y_d^\dagger\right) - 3\lambda_1\mathrm{Tr}\left(Y_d Y_d^\dagger Y_d Y_d^\dagger\right) \\
& - \frac{12}{5}g_1^2\mathrm{Tr}\left(Y_e Y_e^\dagger Y_e Y_e^\dagger\right) - \lambda_1\mathrm{Tr}\left(Y_e Y_e^\dagger Y_e Y_e^\dagger\right) - 14\lambda_1\mathrm{Tr}\left(Y_e Y_N^\dagger Y_N Y_e^\dagger\right) \\
& - \lambda_1\mathrm{Tr}\left(Y_N Y_N^\dagger Y_N Y_N^\dagger\right) - \frac{8}{5}g_1^2\mathrm{Tr}\left(Y_u Y_u^\dagger Y_u Y_u^\dagger\right) - 32g_3^2\mathrm{Tr}\left(Y_u Y_u^\dagger Y_u Y_u^\dagger\right) \\
& - 3\lambda_1\mathrm{Tr}\left(Y_u Y_u^\dagger Y_u Y_u^\dagger\right) - 42\lambda_1\mathrm{Tr}\left(Y_u Y_u^\dagger Y_d^\intercal Y_d^*\right) + 30\mathrm{Tr}\left(Y_d Y_d^\dagger Y_d Y_d^\dagger Y_d Y_d^\dagger\right) \\
& + 10\mathrm{Tr}\left(Y_e Y_e^\dagger Y_e Y_e^\dagger Y_e Y_e^\dagger\right) - 4\mathrm{Tr}\left(Y_e Y_e^\dagger Y_e Y_N^\dagger Y_N Y_e^\dagger\right) + 2\mathrm{Tr}\left(Y_e Y_N^\dagger Y_N Y_e^\dagger Y_e Y_e^\dagger\right) \\
& + 10\mathrm{Tr}\left(Y_N Y_N^\dagger Y_N Y_N^\dagger Y_N Y_N^\dagger\right) + 30\mathrm{Tr}\left(Y_u Y_u^\dagger Y_u Y_u^\dagger Y_u Y_u^\dagger\right) - 6\mathrm{Tr}\left(Y_u Y_u^\dagger Y_u Y_u^\dagger Y_d^\intercal Y_d^*\right) \\
& - 6\mathrm{Tr}\left(Y_u Y_u^\dagger Y_d^\intercal Y_d^* Y_d^\intercal Y_d^*\right) - 2\mathrm{Tr}\left(Y_e Y_N^\dagger Y_N Y_N^\dagger Y_N Y_e^\dagger\right)\Bigg].
\end{aligned}
$$

$$\beta_{\lambda_2} = \frac{1}{16\pi^2}\left[24\lambda_2^2 + 2\lambda_3^2 + 2\lambda_3\lambda_4 + 4\lambda_5^2 - 9g_2^2\lambda_2 + \frac{27}{200}g_1^4 + \frac{9}{20}g_1^2\left(-4\lambda_2 + g_2^2\right) + \frac{9}{8}g_2^4 + \lambda_4^2\right]$$

$$+ \frac{1}{(16\pi^2)^2}\left[-\frac{3537}{2000}g_1^6 - \frac{1719}{400}g_1^4g_2^2 - \frac{303}{80}g_1^2g_2^4 + \frac{291}{16}g_2^6 + \frac{1953}{200}g_1^4\lambda_2 + \frac{117}{20}g_1^2g_2^2\lambda_2 - \frac{51}{8}g_2^4\lambda_2\right.$$

$$+ \frac{108}{5}g_1^2\lambda_2^2 + 108g_2^2\lambda_2^2 - 312\lambda_2^3 + \frac{9}{10}g_1^4\lambda_3 + \frac{15}{2}g_2^4\lambda_3 + \frac{12}{5}g_1^2\lambda_3^2 + 12g_2^2\lambda_3^2 - 20\lambda_2\lambda_3^2$$

$$- 8\lambda_3^3 + \frac{9}{20}g_1^4\lambda_4 - \frac{3}{2}g_1^2g_2^2\lambda_4 + \frac{15}{4}g_2^4\lambda_4 + \frac{12}{5}g_1^2\lambda_3\lambda_4 + 12g_2^2\lambda_3\lambda_4 - 20\lambda_2\lambda_3\lambda_4$$

$$- 12\lambda_3^2\lambda_4 + \frac{6}{5}g_1^2\lambda_4^2 + 3g_2^2\lambda_4^2 - 12\lambda_2\lambda_4^2 - 16\lambda_3\lambda_4^2 - 6\lambda_4^3 - \frac{12}{5}g_1^2\lambda_5^2 - 56\lambda_2\lambda_5^2$$

$$- 80\lambda_3\lambda_5^2 + 8\lambda_4\lambda_5^2 - 6\left(2\lambda_3^2 + 2\lambda_3\lambda_4 + 4\lambda_5^2 + \lambda_4^2\right)\mathrm{Tr}\left(Y_dY_d^\dagger\right)$$

$$- 2\left(2\lambda_3^2 + 2\lambda_3\lambda_4 + 4\lambda_5^2 + \lambda_4^2\right)\mathrm{Tr}\left(Y_eY_e^\dagger\right) - 4\lambda_3^2\mathrm{Tr}\left(Y_NY_N^\dagger\right) - 4\lambda_3\lambda_4\mathrm{Tr}\left(Y_NY_N^\dagger\right)$$

$$- 2\lambda_4^2\mathrm{Tr}\left(Y_NY_N^\dagger\right) - 8\lambda_5^2\mathrm{Tr}\left(Y_NY_N^\dagger\right) - 12\lambda_3^2\mathrm{Tr}\left(Y_uY_u^\dagger\right) - 12\lambda_3\lambda_4\mathrm{Tr}\left(Y_uY_u^\dagger\right)$$

$$\left.- 6\lambda_4^2\mathrm{Tr}\left(Y_uY_u^\dagger\right) - 24\lambda_5^2\mathrm{Tr}\left(Y_uY_u^\dagger\right)\right].$$

$$\beta_{\lambda_3} = \frac{1}{16\pi^2}\left[\frac{27}{100}g_1^4 + \frac{9}{10}g_1^2g_2^2 + \frac{9}{4}g_2^4 - \frac{9}{5}g_1^2\lambda_3 - 9g_2^2\lambda_3 + 12\lambda_1\lambda_3 + 12\lambda_2\lambda_3 + 4\lambda_3^2 + 4\lambda_1\lambda_4 + 4\lambda_2\lambda_4\right.$$

$$\left.+ 2\lambda_4^2 + 40\lambda_5^2 + 6\lambda_3\mathrm{Tr}\left(Y_dY_d^\dagger\right) + 2\lambda_3\mathrm{Tr}\left(Y_eY_e^\dagger\right) + 2\lambda_3\mathrm{Tr}\left(Y_NY_N^\dagger\right) + 6\lambda_3\mathrm{Tr}\left(Y_uY_u^\dagger\right)\right]$$

$$+ \frac{1}{(16\pi^2)^2}\left[-\frac{3537}{1000}g_1^6 - \frac{1719}{200}g_1^4g_2^2 - \frac{303}{40}g_1^2g_2^4 + \frac{291}{8}g_2^6 + \frac{27}{10}g_1^4\lambda_1 + 3g_1^2g_2^2\lambda_1 + \frac{45}{2}g_2^4\lambda_1\right.$$

$$+ \frac{27}{10}g_1^4\lambda_2 + 3g_1^2g_2^2\lambda_2 + \frac{45}{2}g_2^4\lambda_2 + \frac{1773}{200}g_1^4\lambda_3 + \frac{57}{20}g_1^2g_2^2\lambda_3 - \frac{111}{8}g_2^4\lambda_3 + \frac{72}{5}g_1^2\lambda_1\lambda_3$$

$$+ 72g_2^2\lambda_1\lambda_3 - 60\lambda_1^2\lambda_3 + \frac{72}{5}g_1^2\lambda_2\lambda_3 + 72g_2^2\lambda_2\lambda_3 - 60\lambda_2^2\lambda_3 + \frac{6}{5}g_1^2\lambda_3^2 + 6g_2^2\lambda_3^2$$

$$- 72\lambda_1\lambda_3^2 - 72\lambda_2\lambda_3^2 - 12\lambda_3^3 + \frac{9}{10}g_1^4\lambda_4 - 3g_1^2g_2^2\lambda_4 + \frac{15}{2}g_2^4\lambda_4 + \frac{24}{5}g_1^2\lambda_1\lambda_4 + 36g_2^2\lambda_1\lambda_4$$

$$- 16\lambda_1^2\lambda_4 + \frac{24}{5}g_1^2\lambda_2\lambda_4 + 36g_2^2\lambda_2\lambda_4 - 16\lambda_2^2\lambda_4 - 12g_2^2\lambda_3\lambda_4 - 32\lambda_1\lambda_3\lambda_4 - 32\lambda_2\lambda_3\lambda_4$$

$$- 4\lambda_3^2\lambda_4 + \frac{12}{5}g_1^2\lambda_4^2 + 6g_2^2\lambda_4^2 - 28\lambda_1\lambda_4^2 - 28\lambda_2\lambda_4^2 - 16\lambda_3\lambda_4^2 - 12\lambda_4^3 + 48g_1^2\lambda_5^2$$

$$+ 216g_2^2\lambda_5^2 - 336\lambda_1\lambda_5^2 - 336\lambda_2\lambda_5^2 - 264\lambda_3\lambda_5^2 + 16\lambda_4\lambda_5^2 - \frac{3}{4}g_2^4\mathrm{Tr}\left(Y_NY_N^\dagger\right)$$

$$+ \frac{3}{4}g_1^2\lambda_3\mathrm{Tr}\left(Y_NY_N^\dagger\right) + \frac{1}{20}\left(-5\left(-45g_2^2\lambda_3 + 8\left(-20g_3^2\lambda_3 + 3\left(20\lambda_5^2 + 2\lambda_3^2\right.\right.\right.\right.$$

$$\left.\left.\left.+ 4\lambda_1\left(3\lambda_3 + \lambda_4\right) + \lambda_4^2\right)\right) + 9g_2^4\right) + 9g_1^4 + g_1^2\left(25\lambda_3 + 54g_2^2\right)\right)\mathrm{Tr}\left(Y_dY_d^\dagger\right)$$

$$- \frac{1}{20}\left(-3g_1^2\left(22g_2^2 + 25\lambda_3\right) + 45g_1^4 + 5\left(-15g_2^2\lambda_3 + 3g_2^4 + 8\left(20\lambda_5^2 + 2\lambda_3^2\right.\right.\right.$$

$$\left.\left.\left.+ 4\lambda_1\left(3\lambda_3 + \lambda_4\right) + \lambda_4^2\right)\right)\right)\mathrm{Tr}\left(Y_eY_e^\dagger\right) - \frac{9}{100}g_1^4\mathrm{Tr}\left(Y_NY_N^\dagger\right) - \frac{3}{10}g_1^2g_2^2\mathrm{Tr}\left(Y_NY_N^\dagger\right)$$

$$+ \frac{15}{4}g_2^2\lambda_3\mathrm{Tr}\left(Y_NY_N^\dagger\right) - 24\lambda_1\lambda_3\mathrm{Tr}\left(Y_NY_N^\dagger\right) - 4\lambda_3^2\mathrm{Tr}\left(Y_NY_N^\dagger\right) - 8\lambda_1\lambda_4\mathrm{Tr}\left(Y_NY_N^\dagger\right)$$

$$- 2\lambda_4^2\mathrm{Tr}\left(Y_NY_N^\dagger\right) - 40\lambda_5^2\mathrm{Tr}\left(Y_NY_N^\dagger\right) - \frac{171}{100}g_1^4\mathrm{Tr}\left(Y_uY_u^\dagger\right) + \frac{63}{10}g_1^2g_2^2\mathrm{Tr}\left(Y_uY_u^\dagger\right)$$

$$- \frac{9}{4}g_2^4\mathrm{Tr}\left(Y_uY_u^\dagger\right) + \frac{17}{4}g_1^2\lambda_3\mathrm{Tr}\left(Y_uY_u^\dagger\right) + \frac{45}{4}g_2^2\lambda_3\mathrm{Tr}\left(Y_uY_u^\dagger\right) + 40g_3^2\lambda_3\mathrm{Tr}\left(Y_uY_u^\dagger\right)$$

$$
\begin{aligned}
&- 72\lambda_1\lambda_3\mathrm{Tr}\left(Y_uY_u^\dagger\right) - 12\lambda_3^2\mathrm{Tr}\left(Y_uY_u^\dagger\right) - 24\lambda_1\lambda_4\mathrm{Tr}\left(Y_uY_u^\dagger\right) - 6\lambda_4^2\mathrm{Tr}\left(Y_uY_u^\dagger\right) \\
&- 120\lambda_5^2\mathrm{Tr}\left(Y_uY_u^\dagger\right) - \frac{27}{2}\lambda_3\mathrm{Tr}\left(Y_dY_d^\dagger Y_dY_d^\dagger\right) - \frac{9}{2}\lambda_3\mathrm{Tr}\left(Y_eY_e^\dagger Y_eY_e^\dagger\right) \\
&- 7\lambda_3\mathrm{Tr}\left(Y_eY_N^\dagger Y_NY_e^\dagger\right) - 8\lambda_4\mathrm{Tr}\left(Y_eY_N^\dagger Y_NY_e^\dagger\right) - \frac{9}{2}\lambda_3\mathrm{Tr}\left(Y_NY_N^\dagger Y_NY_N^\dagger\right) \\
&- \frac{27}{2}\lambda_3\mathrm{Tr}\left(Y_uY_u^\dagger Y_uY_u^\dagger\right) - 21\lambda_3\mathrm{Tr}\left(Y_uY_u^\dagger Y_d^\mathsf{T}Y_d^*\right) - 24\lambda_4\mathrm{Tr}\left(Y_uY_u^\dagger Y_d^\mathsf{T}Y_d^*\right)\bigg] .
\end{aligned}
$$

$$
\begin{aligned}
\beta_{\lambda_4} =\ & \frac{1}{16\pi^2}\bigg[- \frac{9}{5}g_1^2g_2^2 - \frac{9}{5}g_1^2\lambda_4 - 9g_2^2\lambda_4 + 4\lambda_1\lambda_4 + 4\lambda_2\lambda_4 + 8\lambda_3\lambda_4 + 4\lambda_4^2 - 32\lambda_5^2 + 6\lambda_4\mathrm{Tr}\left(Y_dY_d^\dagger\right) \\
& + 2\lambda_4\mathrm{Tr}\left(Y_eY_e^\dagger\right) + 2\lambda_4\mathrm{Tr}\left(Y_NY_N^\dagger\right) + 6\lambda_4\mathrm{Tr}\left(Y_uY_u^\dagger\right)\bigg] \\
& + \frac{1}{(16\pi^2)^2}\bigg[+ \frac{657}{50}g_1^4g_2^2 + \frac{42}{5}g_1^2g_2^4 - 6g_1^2g_2^2\lambda_1 - 6g_1^2g_2^2\lambda_2 - \frac{6}{5}g_1^2g_2^2\lambda_3 + \frac{1413}{200}g_1^4\lambda_4 + \frac{129}{20}g_1^2g_2^2\lambda_4 \\
& - \frac{231}{8}g_2^4\lambda_4 + \frac{24}{5}g_1^2\lambda_1\lambda_4 - 28\lambda_1^2\lambda_4 + \frac{24}{5}g_1^2\lambda_2\lambda_4 - 28\lambda_2^2\lambda_4 + \frac{12}{5}g_1^2\lambda_3\lambda_4 + 36g_2^2\lambda_3\lambda_4 \\
& - 80\lambda_1\lambda_3\lambda_4 - 80\lambda_2\lambda_3\lambda_4 - 28\lambda_3^2\lambda_4 - \frac{12}{5}g_1^2\lambda_4^2 + 18g_2^2\lambda_4^2 - 40\lambda_1\lambda_4^2 - 40\lambda_2\lambda_4^2 - 28\lambda_3\lambda_4^2 \\
& - \frac{192}{5}g_1^2\lambda_5^2 - 216g_2^2\lambda_5^2 + 192\lambda_1\lambda_5^2 + 192\lambda_2\lambda_5^2 + 192\lambda_3\lambda_5^2 + 88\lambda_4\lambda_5^2 + 27\lambda_4\mathrm{Tr}\left(Y_uY_u^\dagger Y_d^\mathsf{T}Y_d^*\right) \\
& + \left(4\left(10g_3^2\lambda_4 - 3\left(2\lambda_1\lambda_4 + 2\lambda_3\lambda_4 - 8\lambda_5^2 + \lambda_4^2\right)\right) + \frac{45}{4}g_2^2\lambda_4 + g_1^2\left(-\frac{27}{5}g_2^2 + \frac{5}{4}\lambda_4\right)\right)\mathrm{Tr}\left(Y_dY_d^\dagger\right) \\
& + \left(-4\left(2\lambda_1\lambda_4 + 2\lambda_3\lambda_4 - 8\lambda_5^2 + \lambda_4^2\right) + \frac{15}{4}g_2^2\lambda_4 + g_1^2\left(\frac{15}{4}\lambda_4 - \frac{33}{5}g_2^2\right)\right)\mathrm{Tr}\left(Y_eY_e^\dagger\right) + \frac{3}{5}g_1^2g_2^2\mathrm{Tr}\left(Y_NY_N^\dagger\right) \\
& + \frac{3}{4}g_1^2\lambda_4\mathrm{Tr}\left(Y_NY_N^\dagger\right) + \frac{15}{4}g_2^2\lambda_4\mathrm{Tr}\left(Y_NY_N^\dagger\right) - 8\lambda_1\lambda_4\mathrm{Tr}\left(Y_NY_N^\dagger\right) - 8\lambda_3\lambda_4\mathrm{Tr}\left(Y_NY_N^\dagger\right) \\
& - 4\lambda_4^2\mathrm{Tr}\left(Y_NY_N^\dagger\right) + 32\lambda_5^2\mathrm{Tr}\left(Y_NY_N^\dagger\right) - \frac{63}{5}g_1^2g_2^2\mathrm{Tr}\left(Y_uY_u^\dagger\right) + \frac{17}{4}g_1^2\lambda_4\mathrm{Tr}\left(Y_uY_u^\dagger\right) \\
& + \frac{45}{4}g_2^2\lambda_4\mathrm{Tr}\left(Y_uY_u^\dagger\right) + 40g_3^2\lambda_4\mathrm{Tr}\left(Y_uY_u^\dagger\right) - 24\lambda_1\lambda_4\mathrm{Tr}\left(Y_uY_u^\dagger\right) - 24\lambda_3\lambda_4\mathrm{Tr}\left(Y_uY_u^\dagger\right) \\
& - 12\lambda_4^2\mathrm{Tr}\left(Y_uY_u^\dagger\right) + 96\lambda_5^2\mathrm{Tr}\left(Y_uY_u^\dagger\right) - \frac{27}{2}\lambda_4\mathrm{Tr}\left(Y_dY_d^\dagger Y_dY_d^\dagger\right) - \frac{9}{2}\lambda_4\mathrm{Tr}\left(Y_eY_e^\dagger Y_eY_e^\dagger\right) \\
& + 9\lambda_4\mathrm{Tr}\left(Y_eY_N^\dagger Y_NY_e^\dagger\right) - \frac{9}{2}\lambda_4\mathrm{Tr}\left(Y_NY_N^\dagger Y_NY_N^\dagger\right) - \frac{27}{2}\lambda_4\mathrm{Tr}\left(Y_uY_u^\dagger Y_uY_u^\dagger\right)\bigg] .
\end{aligned}
$$

$$
\begin{aligned}
\beta_{\lambda_5} =\ & \frac{1}{16\pi^2}\bigg[- \frac{9}{5}g_1^2\lambda_5 - 9g_2^2\lambda_5 + 4\lambda_1\lambda_5 + 4\lambda_2\lambda_5 + 8\lambda_3\lambda_5 - 4\lambda_4\lambda_5 \\
& + 6\lambda_5\mathrm{Tr}\left(Y_dY_d^\dagger\right) + 2\lambda_5\mathrm{Tr}\left(Y_eY_e^\dagger\right) + 2\lambda_5\mathrm{Tr}\left(Y_NY_N^\dagger\right) + 6\lambda_5\mathrm{Tr}\left(Y_uY_u^\dagger\right)\bigg] \\
& + \frac{1}{(16\pi^2)^2}\bigg[\frac{1413}{200}g_1^4\lambda_5 + \frac{57}{20}g_1^2g_2^2\lambda_5 - \frac{231}{8}g_2^4\lambda_5 - \frac{12}{5}g_1^2\lambda_1\lambda_5 - 28\lambda_1^2\lambda_5 - \frac{12}{5}g_1^2\lambda_2\lambda_5 - 28\lambda_2^2\lambda_5 \\
& + \frac{48}{5}g_1^2\lambda_3\lambda_5 + 36g_2^2\lambda_3\lambda_5 - 80\lambda_1\lambda_3\lambda_5 - 80\lambda_2\lambda_3\lambda_5 - 28\lambda_3^2\lambda_5 - \frac{24}{5}g_1^2\lambda_4\lambda_5 - 36g_2^2\lambda_4\lambda_5 \\
& + 8\lambda_1\lambda_4\lambda_5 + 8\lambda_2\lambda_4\lambda_5 + 20\lambda_3\lambda_4\lambda_5 + 16\lambda_4^2\lambda_5 + 24\lambda_5^3 + \frac{15}{4}g_2^2\lambda_5\mathrm{Tr}\left(Y_NY_N^\dagger\right) \\
& + \frac{1}{4}\left(16\left(10g_3^2 + 3\lambda_4 - 6\lambda_1 - 6\lambda_3\right) + 45g_2^2 + 5g_1^2\right)\lambda_5\mathrm{Tr}\left(Y_dY_d^\dagger\right) \\
& + \frac{1}{4}\left(15g_1^2 + 15g_2^2 + 16\left(-2\lambda_1 - 2\lambda_3 + \lambda_4\right)\right)\lambda_5\mathrm{Tr}\left(Y_eY_e^\dagger\right) + \frac{3}{4}g_1^2\lambda_5\mathrm{Tr}\left(Y_NY_N^\dagger\right)
\end{aligned}
$$

$$-8\lambda_1\lambda_5\text{Tr}\left(Y_N Y_N^\dagger\right) - 8\lambda_3\lambda_5\text{Tr}\left(Y_N Y_N^\dagger\right) + 4\lambda_4\lambda_5\text{Tr}\left(Y_N Y_N^\dagger\right) + \frac{17}{4}g_1^2\lambda_5\text{Tr}\left(Y_u Y_u^\dagger\right)$$

$$+ \frac{45}{4}g_2^2\lambda_5\text{Tr}\left(Y_u Y_u^\dagger\right) + 40g_3^2\lambda_5\text{Tr}\left(Y_u Y_u^\dagger\right) - 24\lambda_1\lambda_5\text{Tr}\left(Y_u Y_u^\dagger\right) - 24\lambda_3\lambda_5\text{Tr}\left(Y_u Y_u^\dagger\right)$$

$$+ 12\lambda_4\lambda_5\text{Tr}\left(Y_u Y_u^\dagger\right) - \frac{3}{2}\lambda_5\text{Tr}\left(Y_d Y_d^\dagger Y_d Y_d^\dagger\right) - \frac{1}{2}\lambda_5\text{Tr}\left(Y_e Y_e^\dagger Y_e Y_e^\dagger\right) + \lambda_5\text{Tr}\left(Y_e Y_N^\dagger Y_N Y_e^\dagger\right)$$

$$- \frac{1}{2}\lambda_5\text{Tr}\left(Y_N Y_N^\dagger Y_N Y_N^\dagger\right) - \frac{3}{2}\lambda_5\text{Tr}\left(Y_u Y_u^\dagger Y_u Y_u^\dagger\right) + 3\lambda_5\text{Tr}\left(Y_u Y_u^\dagger Y_d^\mathsf{T} Y_d^*\right)\bigg] .$$

A.2   Gauge Couplings

$$\beta_{g_1} = \frac{1}{16\pi^2}\left[\frac{21}{5}g_1^3\right] + \frac{1}{(16\pi^2)^2}\left[\frac{1}{50}g_1^3\left(180g_2^2 + 208g_1^2 + 440g_3^2 - 15\text{Tr}\left(Y_N Y_N^\dagger\right) - 25\text{Tr}\left(Y_d Y_d^\dagger\right)\right.\right.$$

$$\left.\left. - 75\text{Tr}\left(Y_e Y_e^\dagger\right) - 85\text{Tr}\left(Y_u Y_u^\dagger\right)\right)\right] .$$

$$\beta_{g_2} = \frac{1}{16\pi^2}\left[-3g_2^3\right] + \frac{1}{(16\pi^2)^2}\left[\frac{1}{10}g_2^3\left(120g_3^2 + 12g_1^2 + 80g_2^2 - 15\text{Tr}\left(Y_d Y_d^\dagger\right) - 15\text{Tr}\left(Y_u Y_u^\dagger\right)\right.\right.$$

$$\left.\left. - 5\text{Tr}\left(Y_e Y_e^\dagger\right) - 5\text{Tr}\left(Y_N Y_N^\dagger\right)\right)\right] .$$

$$\beta_{g_3} = \frac{1}{16\pi^2}\left[-7g_3^3\right] + \frac{1}{(16\pi^2)^2}\left[-\frac{1}{10}g_3^3\left(-11g_1^2 + 260g_3^2 - 45g_2^2\right.\right.$$

$$\left.\left. + 20\text{Tr}\left(Y_d Y_d^\dagger\right) + 20\text{Tr}\left(Y_u Y_u^\dagger\right)\right)\right] .$$

A.3   Yukawa Coupling

$$\beta_{Y_u} = \frac{1}{16\pi^2}\left[\frac{3}{2}\left(-Y_d^\mathsf{T} Y_d^* Y_u + Y_u Y_u^\dagger Y_u\right) + Y_u\left(3\text{Tr}\left(Y_d Y_d^\dagger\right) + 3\text{Tr}\left(Y_u Y_u^\dagger\right) - 8g_3^2 - \frac{17}{20}g_1^2\right.\right.$$

$$\left.\left. - \frac{9}{4}g_2^2 + \text{Tr}\left(Y_e Y_e^\dagger\right) + \text{Tr}\left(Y_N Y_N^\dagger\right)\right)\right]$$

$$+ \frac{1}{(16\pi^2)^2}\left[\frac{1}{80}\left(20\left(11Y_d^\mathsf{T} Y_d^* Y_d^\mathsf{T} Y_d^* Y_u - 4Y_d^\mathsf{T} Y_d^* Y_u Y_u^\dagger Y_u + 6Y_u Y_u^\dagger Y_u Y_u^\dagger Y_u - Y_u Y_u^\dagger Y_d^\mathsf{T} Y_d^* Y_u\right)\right.\right.$$

$$+ Y_u Y_u^\dagger Y_u\left(1280g_3^2 - 180\text{Tr}\left(Y_e Y_e^\dagger\right) - 180\text{Tr}\left(Y_N Y_N^\dagger\right) + 223g_1^2 - 540\text{Tr}\left(Y_d Y_d^\dagger\right)\right.$$

$$\left. - 540\text{Tr}\left(Y_u Y_u^\dagger\right) + 675g_2^2 - 960\lambda_1\right) + Y_d^\mathsf{T} Y_d^* Y_u\left(100\text{Tr}\left(Y_e Y_e^\dagger\right) + 100\text{Tr}\left(Y_N Y_N^\dagger\right)\right.$$

$$\left. - 1280g_3^2 + 300\text{Tr}\left(Y_d Y_d^\dagger\right) + 300\text{Tr}\left(Y_u Y_u^\dagger\right) - 43g_1^2 + 45g_2^2\right)\right)$$

$$+ Y_u\left(\frac{1267}{600}g_1^4 - \frac{9}{20}g_1^2 g_2^2 - \frac{21}{4}g_2^4 + \frac{19}{15}g_1^2 g_3^2 + 9g_2^2 g_3^2 - 108g_3^4 + 6\lambda_1^2 + \lambda_3^2 + \lambda_3\lambda_4\right.$$

$$+ \lambda_4^2 + 6\lambda_5^2 + \frac{5}{8}\left(32g_3^2 + 9g_2^2 + g_1^2\right)\text{Tr}\left(Y_d Y_d^\dagger\right) + \frac{15}{8}\left(g_1^2 + g_2^2\right)\text{Tr}\left(Y_e Y_e^\dagger\right)$$

$$+ \frac{3}{8}g_1^2\text{Tr}\left(Y_N Y_N^\dagger\right) + \frac{15}{8}g_2^2\text{Tr}\left(Y_N Y_N^\dagger\right) + \frac{17}{8}g_1^2\text{Tr}\left(Y_u Y_u^\dagger\right) + \frac{45}{8}g_2^2\text{Tr}\left(Y_u Y_u^\dagger\right)$$

$$+ 20g_3^2\text{Tr}\left(Y_u Y_u^\dagger\right) - \frac{27}{4}\text{Tr}\left(Y_d Y_d^\dagger Y_d Y_d^\dagger\right) - \frac{9}{4}\text{Tr}\left(Y_e Y_e^\dagger Y_e Y_e^\dagger\right) + \frac{1}{2}\text{Tr}\left(Y_e Y_N^\dagger Y_N Y_e^\dagger\right)$$

$$- \frac{9}{4}\text{Tr}\left(Y_N Y_N^\dagger Y_N Y_N^\dagger\right) - \frac{27}{4}\text{Tr}\left(Y_u Y_u^\dagger Y_u Y_u^\dagger\right) + \frac{3}{2}\text{Tr}\left(Y_u Y_u^\dagger Y_d^\mathsf{T} Y_d^*\right)\right)\bigg] .$$

References

[1] G. Aad *et al.* [ATLAS Collaboration], Phys. Lett. B **716**, 1 (2012) [arXiv:1207.7214 [hep-ex]].

[2] S. Chatrchyan *et al.* [CMS Collaboration], Phys. Lett. B **716**, 30 (2012) [arXiv:1207.7235 [hep-ex]].

[3] G. Aad *et al.* [ATLAS Collaboration], Phys. Lett. B **726**, 120 (2013) [arXiv:1307.1432 [hep-ex]].

[4] V. Khachatryan *et al.* [CMS Collaboration], Phys. Rev. D **92**, no. 1, 012004 (2015) [arXiv:1411.3441 [hep-ex]].

[5] A. M. Sirunyan *et al.* [CMS Collaboration], Eur. Phys. J. C **79**, no. 5, 421 (2019) [arXiv:1809.10733 [hep-ex]].

[6] G. Aad *et al.* [ATLAS Collaboration], arXiv:1909.02845 [hep-ex].

[7] A. Djouadi, Phys. Rept. **457**, 1 (2008) [hep-ph/0503172].

[8] G. Isidori, G. Ridolfi and A. Strumia, Nucl. Phys. B **609**, 387 (2001) [hep-ph/0104016].

[9] F. Bezrukov, M. Y. Kalmykov, B. A. Kniehl and M. Shaposhnikov, JHEP **1210**, 140 (2012) [arXiv:1205.2893 [hep-ph]].

[10] G. Degrassi, S. Di Vita, J. Elias-Miro, J. R. Espinosa, G. F. Giudice, G. Isidori and A. Strumia, JHEP **1208**, 098 (2012) [arXiv:1205.6497 [hep-ph]].

[11] D. Buttazzo, G. Degrassi, P. P. Giardino, G. F. Giudice, F. Sala, A. Salvio and A. Strumia, JHEP **1312**, 089 (2013) [arXiv:1307.3536 [hep-ph]].

[12] M. Tanabashi *et al.* [Particle Data Group], Phys. Rev. D **98**, no. 3, 030001 (2018).

[13] T. Markkanen, A. Rajantie and S. Stopyra, Front. Astron. Space Sci. **5**, 40 (2018) [arXiv:1809.06923 [astro-ph.CO]].

[14] F. L. Bezrukov and M. Shaposhnikov, Phys. Lett. B **659**, 703 (2008) [arXiv:0710.3755 [hep-th]].

[15] F. Bezrukov, J. Rubio and M. Shaposhnikov, Phys. Rev. D **92**, no. 8, 083512 (2015) [arXiv:1412.3811 [hep-ph]].

[16] V. Branchina and E. Messina, Phys. Rev. Lett. **111**, 241801 (2013) [arXiv:1307.5193 [hep-ph]].

[17] Z. Lalak, M. Lewicki and P. Olszewski, JHEP **1405**, 119 (2014) [arXiv:1402.3826 [hep-ph]].

[18] V. Branchina, E. Messina and M. Sher, Phys. Rev. D **91**, 013003 (2015) [arXiv:1408.5302 [hep-ph]].

[19] M. Gonderinger, Y. Li, H. Patel and M. J. Ramsey-Musolf, JHEP **1001**, 053 (2010) [arXiv:0910.3167 [hep-ph]].

[20] M. Gonderinger, H. Lim and M. J. Ramsey-Musolf, Phys. Rev. D **86**, 043511 (2012) [arXiv:1202.1316 [hep-ph]].

[21] O. Lebedev, Eur. Phys. J. C **72**, 2058 (2012) [arXiv:1203.0156 [hep-ph]].

[22] J. Elias-Miro, J. R. Espinosa, G. F. Giudice, H. M. Lee and A. Strumia, JHEP **1206**, 031 (2012) [arXiv:1203.0237 [hep-ph]].

[23] C. Balazs, A. Fowlie, A. Mazumdar and G. White, Phys. Rev. D **95**, no. 4, 043505 (2017) [arXiv:1611.01617 [hep-ph]].

[24] P. Athron, J. M. Cornell, F. Kahlhoefer, J. Mckay, P. Scott and S. Wild, Eur. Phys. J. C **78**, no. 10, 830 (2018) [arXiv:1806.11281 [hep-ph]].

[25] P. S. B. Dev, F. Ferrer, Y. Zhang and Y. Zhang, JCAP **1911**, no. 11, 006 (2019) [arXiv:1905.00891 [hep-ph]].

[26] P. M. Ferreira, R. Santos and A. Barroso, Phys. Lett. B **603**, 219 (2004) Erratum: [Phys. Lett. B **629**, 114 (2005)] [hep-ph/0406231].

[27] M. Maniatis, A. von Manteuffel, O. Nachtmann and F. Nagel, Eur. Phys. J. C **48**, 805 (2006) [hep-ph/0605184].

[28] A. Barroso, P. M. Ferreira, R. Santos and J. P. Silva, Phys. Rev. D **74**, 085016 (2006) [hep-ph/0608282].

[29] R. A. Battye, G. D. Brawn and A. Pilaftsis, JHEP **1108**, 020 (2011) [arXiv:1106.3482 [hep-ph]].

[30] K. Kannike, Eur. Phys. J. C **76**, no. 6, 324 (2016) Erratum: [Eur. Phys. J. C **78**, no. 5, 355 (2018)] [arXiv:1603.02680 [hep-ph]].

[31] X. J. Xu, Phys. Rev. D **95**, no. 11, 115019 (2017) [arXiv:1705.08965 [hep-ph]].

[32] I. Gogoladze, N. Okada and Q. Shafi, Phys. Rev. D **78**, 085005 (2008) [arXiv:0802.3257 [hep-ph]].

[33] E. J. Chun, H. M. Lee and P. Sharma, JHEP **1211**, 106 (2012) [arXiv:1209.1303 [hep-ph]].

[34] P. S. B. Dev, D. K. Ghosh, N. Okada and I. Saha, JHEP **1303**, 150 (2013) Erratum: [JHEP **1305**, 049 (2013)] [arXiv:1301.3453 [hep-ph]].

[35] A. Kobakhidze and A. Spencer-Smith, JHEP **1308**, 036 (2013) [arXiv:1305.7283 [hep-ph]].

[36] C. Bonilla, R. M. Fonseca and J. W. F. Valle, Phys. Rev. D **92**, no. 7, 075028 (2015) [arXiv:1508.02323 [hep-ph]].

[37] N. Haba, H. Ishida, N. Okada and Y. Yamaguchi, Eur. Phys. J. C **76**, no. 6, 333 (2016) [arXiv:1601.05217 [hep-ph]].

[38] P. S. B. Dev, C. M. Vila and W. Rodejohann, Nucl. Phys. B **921**, 436 (2017) [arXiv:1703.00828 [hep-ph]].

[39] A. Datta, A. Elsayed, S. Khalil and A. Moursy, Phys. Rev. D **88**, no. 5, 053011 (2013) [arXiv:1308.0816 [hep-ph]].

[40] J. Chakrabortty, P. Konar and T. Mondal, Phys. Rev. D **89**, no. 5, 056014 (2014) [arXiv:1308.1291 [hep-ph]].

[41] C. Coriano, L. Delle Rose and C. Marzo, Phys. Lett. B **738**, 13 (2014) [arXiv:1407.8539 [hep-ph]].

[42] N. Haba and Y. Yamaguchi, PTEP **2015**, no. 9, 093B05 (2015) [arXiv:1504.05669 [hep-ph]].

[43] S. Oda, N. Okada and D. s. Takahashi, Phys. Rev. D **92**, no. 1, 015026 (2015) [arXiv:1504.06291 [hep-ph]].

[44] A. Das, N. Okada and N. Papapietro, Eur. Phys. J. C **77**, no. 2, 122 (2017) [arXiv:1509.01466 [hep-ph]].

[45] A. Das, S. Oda, N. Okada and D. s. Takahashi, Phys. Rev. D **93**, no. 11, 115038 (2016) [arXiv:1605.01157 [hep-ph]].

[46] R. N. Mohapatra, Phys. Rev. D **34**, 909 (1986).

[47] P. S. B. Dev, R. N. Mohapatra, W. Rodejohann and X. J. Xu, JHEP **1902**, 154 (2019) [arXiv:1811.06869 [hep-ph]].

[48] G. Chauhan, arXiv:1907.07153 [hep-ph].

[49] R. N. Mohapatra and Y. Zhang, JHEP **1406**, 072 (2014) [arXiv:1401.6701 [hep-ph]].

[50] P. S. B. Dev, R. N. Mohapatra and Y. Zhang, JHEP **1602**, 186 (2016) [arXiv:1512.08507 [hep-ph]].

[51] W. Chao, J. H. Zhang and Y. Zhang, JHEP **1306**, 039 (2013) [arXiv:1212.6272 [hep-ph]].

[52] K. S. Babu, I. Gogoladze and S. Khan, Phys. Rev. D **95**, no. 9, 095013 (2017) [arXiv:1612.05185 [hep-ph]].

[53] J. Sirkka and I. Vilja, Phys. Lett. B **332**, 141 (1994) [hep-ph/9404268].

[54] C. Bonilla, R. M. Fonseca and J. W. F. Valle, Phys. Lett. B **756**, 345 (2016) [arXiv:1506.04031 [hep-ph]].

[55] A. Masoumi and A. Vilenkin, JCAP **1603**, 054 (2016) [arXiv:1601.01662 [gr-qc]].

[56] M. Rummel and Y. Sumitomo, JHEP **1312**, 003 (2013) [arXiv:1310.4202 [hep-th]].

[57] Y. Ema, K. Mukaida and K. Nakayama, Phys. Lett. B **761**, 419 (2016) [arXiv:1605.07342 [hep-ph]].

[58] P. Bandyopadhyay and R. Mandal, Phys. Rev. D **95** (2017) no.3, 035007 [arXiv:1609.03561 [hep-ph]].

[59] X. G. He, H. Phoon, Y. Tang and G. Valencia, JHEP **1305**, 026 (2013) [arXiv:1303.4848 [hep-ph]].

[60] M. Heikinheimo, K. Kannike, F. Lyonnet, M. Raidal, K. Tuominen and H. VeermÃďe, JHEP **1710**, 014 (2017) [arXiv:1707.08980 [hep-ph]].

[61] T. L. Curtright and G. I. Ghandour, Phys. Lett. **59B**, 387 (1975).

[62] E. Gabrielli, K. Huitu and S. Roy, Phys. Rev. D **65**, 075005 (2002) [hep-ph/0108246].

[63] A. Datta and X. Zhang, Int. J. Mod. Phys. A **21**, 2431 (2006) [hep-ph/0412255].

[64] J. L. Evans, D. E. Morrissey and J. D. Wells, Phys. Rev. D **80**, 095011 (2009) [arXiv:0812.3874 [hep-ph]].

[65] G. F. Giudice and A. Strumia, Nucl. Phys. B **858**, 63 (2012) [arXiv:1108.6077 [hep-ph]].

[66] J. E. Camargo-Molina, B. O'Leary, W. Porod and F. Staub, JHEP **1312**, 103 (2013) [arXiv:1309.7212 [hep-ph]].

[67] L. Basso, B. Fuks, M. E. Krauss and W. Porod, JHEP **1507**, 147 (2015) [arXiv:1503.08211 [hep-ph]].

[68] E. Bagnaschi, F. BrÃijmmer, W. BuchmÃijller, A. Voigt and G. Weiglein, JHEP **1603**, 158 (2016) [arXiv:1512.07761 [hep-ph]].

[69] V. S. Mummidi, V. P. K. and K. M. Patel, JHEP **1808**, 134 (2018) [arXiv:1805.08005 [hep-ph]].

[70] F. Staub, Phys. Lett. B **789**, 203 (2019) [arXiv:1811.08300 [hep-ph]].

[71] W. Ahmed, A. Mansha, T. Li, S. Raza, J. Roy and F. Z. Xu, arXiv:1901.05278 [hep-ph].

[72] J. A. Casas, V. Di Clemente, A. Ibarra and M. Quiros, Phys. Rev. D **62**, 053005 (2000) [hep-ph/9904295].

[73] J. Elias-Miro, J. R. Espinosa, G. F. Giudice, G. Isidori, A. Riotto and A. Strumia, Phys. Lett. B **709**, 222 (2012) [arXiv:1112.3022 [hep-ph]].

[74] W. Rodejohann and H. Zhang, JHEP **1206**, 022 (2012) [arXiv:1203.3825 [hep-ph]].

[75] I. Masina, Phys. Rev. D **87**, no. 5, 053001 (2013) [arXiv:1209.0393 [hep-ph]].

[76] M. Farina, D. Pappadopulo and A. Strumia, JHEP **1308**, 022 (2013) [arXiv:1303.7244 [hep-ph]].

[77] J. N. Ng and A. de la Puente, Eur. Phys. J. C **76**, no. 3, 122 (2016) [arXiv:1510.00742 [hep-ph]].

[78] G. Bambhaniya, P. S. B. Dev, S. Goswami, S. Khan and W. Rodejohann, Phys. Rev. D **95**, no. 9, 095016 (2017) [arXiv:1611.03827 [hep-ph]].

[79] I. Gogoladze, N. Okada and Q. Shafi, Phys. Lett. B **668**, 121 (2008) [arXiv:0805.2129 [hep-ph]].

[80] C. S. Chen and Y. Tang, JHEP **1204**, 019 (2012) [arXiv:1202.5717 [hep-ph]].

[81] M. Lindner, H. H. Patel and B. Radovčić, Phys. Rev. D **93**, no. 7, 073005 (2016) [arXiv:1511.06215 [hep-ph]].

[82] S. Goswami, K. N. Vishnudath and N. Khan, Phys. Rev. D **99**, no. 7, 075012 (2019) [arXiv:1810.11687 [hep-ph]].

[83] S. Khan, S. Goswami and S. Roy, Phys. Rev. D **89**, no. 7, 073021 (2014) [arXiv:1212.3694 [hep-ph]].

[84] L. Delle Rose, C. Marzo and A. Urbano, JHEP **1512**, 050 (2015) [arXiv:1506.03360 [hep-ph]].

[85] A. Das, S. Goswami, K. N. Vishnudath and T. Nomura, arXiv:1905.00201 [hep-ph].

[86] S. Baek, P. Ko, W. I. Park and E. Senaha, JHEP **1211**, 116 (2012) [arXiv:1209.4163 [hep-ph]].

[87] M. Lindner, M. Platscher, C. E. Yaguna and A. Merle, Phys. Rev. D **94**, no. 11, 115027 (2016) [arXiv:1608.00577 [hep-ph]].

[88] A. Dutta Banik, A. K. Saha and A. Sil, Phys. Rev. D **98**, no. 7, 075013 (2018) [arXiv:1806.08080 [hep-ph]].

[89] J. W. Wang, X. J. Bi, P. F. Yin and Z. H. Yu, Phys. Rev. D **99**, no. 5, 055009 (2019) [arXiv:1811.08743 [hep-ph]].

[90] M. L. Xiao and J. H. Yu, Phys. Rev. D **90**, no. 1, 014007 (2014) Addendum: [Phys. Rev. D **90**, no. 1, 019901 (2014)] [arXiv:1404.0681 [hep-ph]].

[91] S. Gopalakrishna and A. Velusamy, Phys. Rev. D **99**, no. 11, 115020 (2019) [arXiv:1812.11303 [hep-ph]].

[92] P. Minkowski, Phys. Lett. **67B**, 421 (1977).

[93] R. N. Mohapatra and G. Senjanovic, Phys. Rev. Lett. **44**, 912 (1980).

[94] T. Yanagida, Conf. Proc. C **7902131**, 95 (1979).

[95] M. Gell-Mann, P. Ramond and R. Slansky, Conf. Proc. C **790927**, 315 (1979) [arXiv:1306.4669 [hep-th]].

[96] J. Schechter and J. W. F. Valle, Phys. Rev. D **22**, 2227 (1980).

[97] P. Ghosh, A. K. Saha and A. Sil, Phys. Rev. D **97**, no. 7, 075034 (2018) [arXiv:1706.04931 [hep-ph]].

[98] I. Garg, S. Goswami, K. N. Vishnudath and N. Khan, Phys. Rev. D **96**, no. 5, 055020 (2017) [arXiv:1706.08851 [hep-ph]].

[99] S. Bhattacharya, P. Ghosh, A. K. Saha and A. Sil, arXiv:1905.12583 [hep-ph].

[100] S. Bhattacharya, N. Chakrabarty, R. Roshan and A. Sil, arXiv:1910.00612 [hep-ph].

[101] N. G. Deshpande and E. Ma, Phys. Rev. D **18**, 2574 (1978).

[102] R. Barbieri, L. J. Hall and V. S. Rychkov, Phys. Rev. D **74**, 015007 (2006) [hep-ph/0603188].

[103] L. Lopez Honorez, E. Nezri, J. F. Oliver and M. H. G. Tytgat, JCAP **0702**, 028 (2007) [hep-ph/0612275].

[104] E. M. Dolle and S. Su, Phys. Rev. D **80**, 055012 (2009) [arXiv:0906.1609 [hep-ph]].

[105] L. Lopez Honorez and C. E. Yaguna, JHEP **1009**, 046 (2010) [arXiv:1003.3125 [hep-ph]].

[106] L. Lopez Honorez and C. E. Yaguna, JCAP **1101**, 002 (2011) [arXiv:1011.1411 [hep-ph]].

[107] A. Goudelis, B. Herrmann and O. Stal, JHEP **1309**, 106 (2013) [arXiv:1303.3010 [hep-ph]].

[108] A. Arhrib, Y. L. S. Tsai, Q. Yuan and T. C. Yuan, JCAP **1406**, 030 (2014) [arXiv:1310.0358 [hep-ph]].

[109] A. Belyaev, G. Cacciapaglia, I. P. Ivanov, F. Rojas-Abatte and M. Thomas, Phys. Rev. D **97**, no. 3, 035011 (2018) [arXiv:1612.00511 [hep-ph]].

[110] G. C. Branco, P. M. Ferreira, L. Lavoura, M. N. Rebelo, M. Sher and J. P. Silva, Phys. Rept. **516**, 1 (2012) [arXiv:1106.0034 [hep-ph]].

[111] A. Atre, T. Han, S. Pascoli and B. Zhang, JHEP **0905**, 030 (2009) [arXiv:0901.3589 [hep-ph]].

[112] F. F. Deppisch, P. S. B. Dev and A. Pilaftsis, New J. Phys. **17**, no. 7, 075019 (2015) [arXiv:1502.06541 [hep-ph]].

[113] J. Kersten and A. Y. Smirnov, Phys. Rev. D **76**, 073005 (2007) [arXiv:0705.3221 [hep-ph]].

[114] X. G. He, S. Oh, J. Tandean and C. C. Wen, Phys. Rev. D **80**, 073012 (2009) [arXiv:0907.1607 [hep-ph]].

[115] R. Adhikari and A. Raychaudhuri, Phys. Rev. D **84**, 033002 (2011) [arXiv:1004.5111 [hep-ph]].

[116] A. Ibarra, E. Molinaro and S. T. Petcov, JHEP **1009**, 108 (2010) [arXiv:1007.2378 [hep-ph]].

[117] M. Mitra, G. Senjanovic and F. Vissani, Nucl. Phys. B **856**, 26 (2012) [arXiv:1108.0004 [hep-ph]].

[118] C. H. Lee, P. S. B. Dev and R. N. Mohapatra, Phys. Rev. D **88**, no. 9, 093010 (2013) [arXiv:1309.0774 [hep-ph]].

[119] P. Chattopadhyay and K. M. Patel, Nucl. Phys. B **921**, 487 (2017) [arXiv:1703.09541 [hep-ph]].

[120] A. E. Cárcamo Hernández, M. González and N. A. Neill, arXiv:1906.00978 [hep-ph].

[121] R. N. Mohapatra, Phys. Rev. Lett. **56**, 561 (1986).

[122] R. N. Mohapatra and J. W. F. Valle, Phys. Rev. D **34**, 1642 (1986).

[123] J. A. Casas and A. Ibarra, Nucl. Phys. B **618**, 171 (2001) [hep-ph/0103065].

[124] F. Staub, Comput. Phys. Commun. **185**, 1773 (2014) [arXiv:1309.7223 [hep-ph]].

[125] F. del Aguila, J. de Blas and M. Perez-Victoria, Phys. Rev. D **78**, 013010 (2008) [arXiv:0803.4008 [hep-ph]].

[126] E. Akhmedov, A. Kartavtsev, M. Lindner, L. Michaels and J. Smirnov, JHEP **1305**, 081 (2013) [arXiv:1302.1872 [hep-ph]].

[127] J. de Blas, EPJ Web Conf. **60**, 19008 (2013) [arXiv:1307.6173 [hep-ph]].

[128] S. Antusch and O. Fischer, JHEP **1410**, 094 (2014) [arXiv:1407.6607 [hep-ph]].

[129] W. Flieger, J. Gluza and K. Porwit, arXiv:1910.01233 [hep-ph].

[130] S. R. Coleman and E. J. Weinberg, Phys. Rev. D **7** (1973) 1888.

[131] J. A. Casas, J. R. Espinosa, M. Quiros and A. Riotto, Nucl. Phys. B **436**, 3 (1995) Erratum: [Nucl. Phys. B **439**, 466 (1995)] [hep-ph/9407389].

[132] N. Khan and S. Rakshit, Phys. Rev. D **92** (2015) 055006 [arXiv:1503.03085 [hep-ph]].

[133] R. Ruiz, M. Spannowsky and P. Waite, Phys. Rev. D **96** (2017) no.5, 055042 [arXiv:1706.02298 [hep-ph]].

[134] A. Belyaev, N. D. Christensen and A. Pukhov, Comput. Phys. Commun. **184** (2013) 1729 [arXiv:1207.6082 [hep-ph]].

[135] R. D. Ball *et al.* [NNPDF Collaboration], JHEP **1504** (2015) 040 [arXiv:1410.8849 [hep-ph]].

[136] A. Abada *et al.* [FCC Collaboration], Eur. Phys. J. ST **228**, no. 4, 755 (2019).

[137] A. Belyaev, G. Cacciapaglia, I. P. Ivanov, F. Rojas-Abatte and M. Thomas, Phys. Rev. D **97** (2018) no.3, 035011 [arXiv:1612.00511 [hep-ph]].

[138] L. Basso, A. Belyaev, S. Moretti and C. H. Shepherd-Themistocleous, Phys. Rev. D **80**, 055030 (2009) [arXiv:0812.4313 [hep-ph]].

[139] Z. Kang, P. Ko and J. Li, Phys. Rev. D **93**, no. 7, 075037 (2016) [arXiv:1512.08373 [hep-ph]].

[140] P. Cox, C. Han and T. T. Yanagida, JHEP **1801**, 037 (2018) [arXiv:1707.04532 [hep-ph]].

[141] A. Das, N. Okada and D. Raut, Eur. Phys. J. C **78**, no. 9, 696 (2018) [arXiv:1711.09896 [hep-ph]].

[142] A. Das, P. S. B. Dev and N. Okada, Phys. Lett. B **799**, 135052 (2019) [arXiv:1906.04132 [hep-ph]].

[143] P. Bandyopadhyay, E. J. Chun and J. C. Park, JHEP **1106** (2011) 129 [arXiv:1105.1652 [hep-ph]].

[144] P. Ko, Y. Omura and C. Yu, JHEP **1401** (2014) 016 [arXiv:1309.7156 [hep-ph]].

[145] P. Bandyopadhyay and E. J. Chun, JHEP **1505** (2015) 045 [arXiv:1412.7312 [hep-ph]].

[146] P. Bandyopadhyay, JHEP **1709** (2017) 052 [arXiv:1511.03842 [hep-ph]].

[147] P. Bandyopadhyay, E. J. Chun and R. Mandal, Phys. Rev. D **97** (2018) no.1, 015001 [arXiv:1707.00874 [hep-ph]].

[148] R. Foot, H. Lew, X. G. He and G. C. Joshi, Z. Phys. C **44** (1989) 441.

[149] P. Bandyopadhyay, S. Choubey and M. Mitra, JHEP **0910** (2009) 012 [arXiv:0906.5330 [hep-ph]].

[150] R. Franceschini, T. Hambye and A. Strumia, Phys. Rev. D **78** (2008) 033002 [arXiv:0805.1613 [hep-ph]].

[151] P. Bandyopadhyay, S. Choi, E. J. Chun and K. Min, Phys. Rev. D **85** (2012) 073013 [arXiv:1112.3080 [hep-ph]].

[152] P. Bandyopadhyay, E. J. Chun, H. Okada and J. C. Park, JHEP **1301** (2013) 079 [arXiv:1209.4803 [hep-ph]].

[153] P. Bandyopadhyay, E. J. Chun and R. Mandal, JHEP **1908** (2019) 169 [arXiv:1904.09494 [hep-ph]].